Interleukin-17 drives sex-dependent weight loss and changes in feeding behaviour during *Trypanosoma brucei* infection

Matthew C. Sinton[1,2¶*], Alex Girard[1,2], John Ogunsola[1,2], Praveena Chandrasegaran[1,2], Paul Capewell[1,2], Georgia Perona-Wright[1,3], Dieudonné M. Ngoyi[4,5], Nono Kuispond[4,5], Bruno Bucheton[5,6], Mamadou Camara[5,7], Shingo Kajimura[8,9], Cécile Bénézech[10], Annette MacLeod[1,2,5¶], Juan F. Quintana[1,2¶*]

[1]Wellcome Centre for Integrative Parasitology, University of Glasgow, Glasgow, UK. [2]School of Biodiversity, One Health and Veterinary Medicine, University of Glasgow, Glasgow, UK. [3]School of Infection and Immunity, University of Glasgow, Glasgow, UK. [4]Department of Parasitology, National Institute of Biomedical Research, Kinshasa, Democratic Republic of Congo. [5]Member of TrypanoGEN. [6]Institut de Recherche pour le Développement, Unité Mixte de Recherche IRD-CIRAD 177, Campus International de Baillarguet, Montpellier, France. [7]Programme National de Lutte contre la Trypanosomiase Humaine Africaine, Ministère de la Santé, Conakry, Guinea. [8]Division of Endocrinology, Diabetes and Metabolism, Beth Israel Deaconess Medical Center and Harvard Medical School, Boston, Massachusetts, USA. [9]Howard Hughes Medical Institute, Chevy Chase, Maryland, USA. [10]Centre for Cardiovascular Science, University of Edinburgh, Edinburgh, EH16 4TJ, Scotland, UK

¶These authors contributed equally to this work

*Corresponding authors

Email: matthew.sinton@glasgow.ac.uk (MCS), juan.quintana@glasgow.ac.uk (JFQ)

Abstract

Previous work has demonstrated that *Trypanosoma brucei* occupy several adipose tissue depots, including the subcutaneous adipose tissue in mice and humans, and due to its proximity to the skin, it is proposed to be an important for transmission. Here, we demonstrate that parasites in the inguinal white adipose tissue (iWAT) niche induce sexually dimorphic responses. During infection, male mice experience reduced adipose tissue mass, altered tissue function, and changes in feeding behaviour, whereas females do not. This tissue impairment correlates with an accumulation of T_H17 T cells in the iWAT. Genetic ablation of IL-17A/F abolishes infection-associated weight loss and alters feeding behaviour, limiting tissue wasting in male mice. Importantly, we detected a significant elevation in serum IL-17A in sleeping sickness patients, indicating that IL-17A/F signalling is also conserved in humans. We propose a model whereby IL-17A/F acts locally in adipocytes *via* engagement with its cognate receptor leading to lipolysis and tissue wasting, and/or systemically, *via* signalling in the hypothalamus to modulate feeding behaviour. Together, our findings suggest key sex-dependent roles for IL-17A/F in regulating adipose tissue and energy balance, as well as a coordinator of brain-adipose tissue communication during sleeping sickness, opening new directions to understand energy balance during infection.

56 **Introduction**

57 *Trypanosoma brucei* is an extracellular protozoan parasite that infects humans and
58 livestock, causing Human African Trypanosomiasis (HAT, or sleeping sickness) and Animal
59 African Trypanosomiasis (AAT, or nagana), respectively (Kennedy, 2019). Both HAT and AAT
60 are prevalent in sub-Saharan regions of the African continent, where they impose a significant
61 socio-economic burden, and are fatal if left untreated (Bukachi et al., 2017). Chronic infections
62 in both humans and non-primate mammalian hosts, such as domestic cattle, lead to significant
63 weight loss, a phenomenon that remains largely unstudied (Kennedy, 2013).

64 Upon infection, trypanosomes proliferate and migrate into tissues throughout the body,
65 where they persist and form extravascular reservoirs in virtually every organ (Malvy and
66 Chappuis, 2011). One major consequence of infection is weight loss, typically coupled with a
67 reduction in adipose tissue mass, referred to as "tissue wasting" (Baazim et al., 2022).
68 Previous studies have elegantly shown that male mice lose weight during *T. brucei* infection
69 and that this is associated with wasting of the gonadal white adipose tissue (gWAT) (Trindade
70 et al., 2016). Indeed, during the course of infection, *T. brucei* forms a reservoir in the gWAT,
71 leading to an expansion of immune cells within the tissue, including macrophages, neutrophils,
72 T helper (T_H)1 cells, effector $CD8^+$ cytotoxic T cells, and B cells (Hube and Hauner, 1999;
73 Machado et al., 2021; Zúñiga et al., 2010), suggesting that adipose tissue wasting might be
74 driven by the parasites, the immune response against them, or both.

75 Adipose tissue is also influenced by immune-derived factors under normal
76 physiological conditions; For example, tumour necrosis factor (TNF) and interleukin-17A (IL-
77 17A) have been shown to regulate adipose tissue structure and function, limiting tissue
78 expansion (Hube and Hauner, 1999), and promoting adipogenesis (Zúñiga et al., 2010),
79 respectively. Furthermore, IL-17A, and signalling through the IL-17C receptor, have been
80 shown to induce thermogenesis in white and brown adipose tissue, respectively (Hu et al.,
81 2020; Kohlgruber et al., 2018), and activation of thermogenesis, following challenges such as
82 cold exposure, leads to increased energy expenditure (van Marken Lichtenbelt and
83 Schrauwen, 2011). IL-17 has also been shown to play a role in controlling resistance to *T.*

84 *cruzi* infection (Guedes et al., 2010), which also leads to weight loss in humans (Cabalén et
85 al., 2016). Furthermore, IL-17 was demonstrated to improve control of parasitaemia in female
86 mice during infection with *T. congloense* (Mou et al., 2010), the parasite responsible for
87 causing AAT. However, it remains unclear how the immune response to *T. brucei* infection
88 influences adipose tissue structure and function.

89 Previous studies from our lab identified the skin as another reservoir for *T. brucei* and
90 highlighted the presence of parasites in the adjacent subcutaneous white adipose tissue
91 (scWAT) of infected patients (Capewell et al., 2016). Due to its proximity to the skin, we
92 focused on understanding the impact of infection on the structure and function of the inguinal
93 white adipose tissue (iWAT) in mice, which is traditionally used to model scWAT in humans
94 (Chusyd et al., 2016). Like gWAT, the iWAT acts as an energy reservoir under homeostatic
95 conditions and modulates systemic metabolism and appetite (Choe et al., 2016) . During times
96 of nutrient deficiency, such as during food deprivation, iWAT increases lipolysis to release
97 nutrients to maintain homeostasis of the organism, leading to tissue remodelling and size
98 reduction (Finn and Dice, 2006). Infection also places a high energy demand on the host, due
99 to activation of the immune response, and if this demand is not met through the intake of
100 nutrients, then the host will use endogenous energy stores such as the adipose tissue, leading
101 to wasting (Childs et al., 2019). Intriguingly, despite the energetic requirements of the immune
102 response, sickness-induced anorexia is a central feature of infection-induced sickness
103 behaviour (Adelman and Martin, 2009). Whilst this paradoxical behaviour is not yet fully
104 understood, there are indications that it is related to cytokine signalling in the hypothalamus
105 (Aviello et al., 2021).

106 Here we present data demonstrating that *T. brucei* infection is associated with sexually
107 dimorphic immune responses in the adipose tissue and provide evidence that IL-17A/F
108 influences adipose tissue wasting and feeding behaviour. These results provide novel insights
109 into the role of IL-17A/F as a regulator of adipose tissue structure and function and feeding
110 behaviour during infection. Furthermore, these findings support the utility of *T. brucei* infection

models for interrogating the role that IL-17A/F plays in controlling energy balance in other diseases.

Results

Infection with *T. brucei* leads to weight loss in a sex-dependent manner

In both humans and livestock, trypanosome infections are known to cause weight loss, and this has been recapitulated in male mouse models of infection (Trindade et al., 2016). However, direct comparisons have not been made between male and female mice to assess whether infection induces weight loss in a sexually dimorphic manner. To test this, we infected age-matched male and female C57BL/6 mice for a period of 25 days. We first wanted to determine that mice were successfully infected and whether there were differences between the levels of circulating parasites between sexes. Parasitaemia measurements followed a characteristic pattern, with no significant differences between sexes (**Figure 1A**). There were also no significant differences in the clinical scores of the mice (**Figure 1B**). Strikingly, during the course of infection, infected male mice lost significant amounts of bodyweight, whereas there was no significant difference between the weights of naïve and infected female mice (**Figure 1C** and **Figure 1D**). Spleen mass increased similarly in both male and female mice (**Supplementary Figure 1**), suggesting that changes in spleen mass during infection do not explain the differences in males and females.

Weight loss may be explained as a consequence of adipose tissue wasting (Dahlman et al., 2010), as a consequence of changes in feeding behaviour (Aviello et al., 2021), or both. To understand this in more detail, we measured gross food intake as a proxy for feeding behaviour. Over the course of infection, the food intake of infected male mice decreased from the onset of infection until 11 days post-infection (dpi), after which it increased to that of naïve males, before dropping again at 25 dpi (**Figure 1E**). Infected female mice displayed a brief, but non-significant, reduction in food intake at 7 dpi, but otherwise maintained a similar feeding behaviour profile to their wild type counterparts (**Figure 1F**). Taken together, these data suggests that weight loss during experimental trypanosomiasis occurs in a sex-dependent manner and is coupled, in males, to feeding behaviour.

167 ***T. brucei* infection reduces iWAT mass and impairs tissue function**

168 We next explored the impact of *T. brucei* infection on the adipose tissue. In addition to
169 changes in feeding behaviour (Aviello et al., 2021), weight loss is typically associated with
170 reductions in adipose tissue mass (Sun et al., 2020). We were particularly interested in the
171 inguinal white adipose tissue (iWAT), which is analogous to the subcutaneous white adipose
172 tissue beneath the skin in humans, as this constitutes an important parasite niche for disease
173 transmission, especially in asymptomatic carriers (Capewell et al., 2016). In a seminal study,
174 Trindade *et al* (2016) identified that colonisation of the gonadal white adipose tissue (gWAT)
175 is associated with weight loss and reduction in adipose mass (Trindade et al., 2016), but the
176 effect on iWAT, which is distinct from gWAT (**Figure 2A**), was not investigated. We first
177 determined the presence of parasites in the iWAT and gWAT by histological analysis (**Figure**
178 **2B**) and, as expected, detected trypanosomes in both tissues. Next, we quantified
179 trypanosome genomic DNA in the iWAT and gWAT as a proxy for determining parasite
180 density, as previously performed (Machado et al., 2021). This highlighted that in male mice
181 there were fewer parasites in the iWAT compared with the gWAT, but that there were no
182 differences between these depots in females (**Figure 2C**). Together, these data suggest that
183 African trypanosomes also establish infectious niches in the iWAT, proximal to the skin.

184 Following our observations of weight loss and the presence of trypanosomes in the
185 iWAT, we then proceeded to characterise the impact of infection on this adipose tissue depot.
186 When normalised to bodyweight, we found that infection led to a significant reduction in the
187 adipose tissue mass of male mice (**Figure 2D**). Female mice also experienced some reduction
188 in iWAT mass, but this was not significant. This raised the question of whether the reduction
189 in mass is due to a loss of lipid content and reduction in adipocyte size (hypotrophy). To
190 address this, we performed Haematoxylin and Eosin (H&E) staining of iWAT at 25 dpi. Visual
191 assessment of the staining indicated that the iWAT of mice infected with *T. brucei* undergoes
192 hypotrophy, with concurrent infiltration of immune cells (**Figure 2E**). To quantify lipid droplet
193 size, which is a proxy for their lipid content, we used the software Adiposoft (Galarraga et al.,
194 2012), Notably, in naïve animals, the size of lipid droplets was almost indistinguishable

195 between males and females, with lipid droplet area ranging from 50 to 700 μm^2 (**Figure 2F**).
196 In contrast, the size range distribution between infected males and females was more
197 constrained, ranging from 50-100 μm^2 (males) up to 300 μm^2 (females) (**Figure 2G**).
198 Considering the extensive wasting of this tissue, we questioned whether this impacted
199 adipose tissue function. We measured blood glycerol levels as a broad marker of tissue
200 function, as it reflects adipose tissue lipolysis rates throughout the body (Duncan et al., 2007).
201 In both infected male and female mice, the circulating glycerol levels were significantly
202 reduced (**Figure 2H**), although there were no sex-specific differences. The changes in glycerol
203 levels observed in experimental infections were also replicated in the serum of stage II HAT
204 patients from the towns of Boffa, Forécariah and Dubréka in Guinea, suggesting that the
205 adipose tissue dysfunction induced by infection also occurs in humans (**Figure 2I**). Taken
206 together, these findings highlight that *T. brucei* infection is associated with significant iWAT
207 wasting and that this, in turn, is associated with impaired tissue function in both mice and
208 humans. Thus, iWAT wasting could influence systemic metabolism, which, in turn, which may
209 ultimately impact immune cell function.

210 **Colonisation of iWAT by *T. brucei* is characterised by upregulation of $CD4^+$ T_H17 T cell**
211 **related transcripts in males but not in females**

212 To better understand the iWAT response to infection, and to identify potential drivers
213 of tissue wasting, we performed bulk transcriptomics analysis of iWAT harvested at 25 dpi
214 from both sexes and included naïve controls for comparison. Principal component analysis
215 (PCA) revealed high levels of variance between naïve and infected males, but less variance
216 between naïve and infected females (**Figure 3A**), potentially indicating a higher transcriptional
217 response in the iWAT of male mice compared to female mice. Indeed, differential expression
218 analysis revealed upregulation of 2,474 genes with a $\log_2$Fold change >0.5 and an adjusted *p*
219 value of <0.05 that were common to both males and females, in addition to 1,410 male- and
220 668 female-specific gene signatures (**Figure 3B**). Of the 2,474 most of the significantly
221 dysregulated genes (*padj* < 0.01) in both males and female mice, we detected robust

222 transcriptional signatures associated with recruitment and activation of the immune system
223 (**Figure 3C**; e.g. *Lyz2, Slamf8, Aif1, Calhm6, Gzmb, Klra2,* and *Clec12a*).
224 Based on the observed adipose tissue wasting, we hypothesised that adipocyte
225 hypotrophy is driven by increased rates of fatty acid oxidation and overall upregulation of
226 energy metabolism. However, using pathway enrichment analysis, we found extensive
227 downregulation of genes related to mitochondrial carbon (including *Idh1*, *Sdha*, *Mdh1*, and
228 subunits of NADH:ubiquinone oxidoreductase and ATPase) and lipid metabolism and storage
229 (including *Pnpla2*, *Cpt2*, *Plin1*, *Plin4*, and *Plin5*) (**Supplementary Table 1**). When we
230 performed pathway enrichment analyses on upregulated genes, we identified common gene
231 signatures in both males and females, including genes related to host response to parasitic
232 and viral infections (leishmaniasis and SARS-CoV-2), including *Ifng*, *Il1b Tlr4*, and *Nlrp3*
233 (**Supplementary Table 2**).
234 Next, we sought to understand which gene pathways are discriminatory between male
235 and female mice. Pathway enrichment analysis of genes exclusively upregulated in females
236 highlighted genes related to folate metabolism (including *Mocs1*, *Mocos*, and *Dhfr*), and
237 protein processing in the endoplasmic reticulum (including *Ero1*, *Pdia4*, and *Pdia6*)
238 (**Supplementary Table 2**). In contrast, several immune-related pathways were exclusively
239 upregulated in males during infection, including those related to T cell signalling and T helper
240 (T_H) cell differentiation: T_H1, T_H2, and T_H17 cells (**Supplementary Table 2**). Upregulated T_H1-
241 and T_H2-related transcripts included *Nfatc1*, *Cd4*, *Cd3e*, *Runx3,* and *Gata3*, suggesting that
242 T_H1 cells may be a significant contributor to interferon gamma (IFNγ) production during
243 infection in the adipose tissue. Additionally, we also detected a significant upregulation of
244 genes typically associated with differentiation of T_H17 effector cells, including *Irf4*, *Cd4*, *Cd3e*,
245 *Il21r*, and *Il6ra* (**Figure 3D**). Taken together, we conclude that the iWAT of male mice
246 experiences a robust pro-inflammatory response potentially mediated by T_H1 and T_H17
247 effector T cells, whereas the iWAT of infected female mice display transcriptional signatures
248 associated with metabolism and protein synthesis.
249

250 **T_H17 effector T cells accumulate in the adipose tissue during chronic *T. brucei* infection**

251 Based on these observations, we hypothesised that T_H17 cells are important for the
252 adipose immune response to infection. To quantify the different populations of $CD4^+$ T cells,
253 including T_H17 cells, present in the iWAT during chronic *T. brucei* infection, we utilised mass
254 cytometry by time of flight (CyTOF), enabling us to gain as much information as possible from
255 the wasted adipose tissue. Previous studies, exploring the gWAT described an expansion of
256 B cells, macrophages, granulocytes, and T cells (Machado et al., 2021). Using a broad panel,
257 we also measured these immune populations in the iWAT (**Figure 4A**). Strikingly, $CD19^+$ B
258 cells in the iWAT represent a smaller proportion of immune cells in males during infection,
259 compared with naïve animals (**Figure 4B**). In contrast, in females, the proportion of iWAT
260 $CD19^+$ B cells remains unaltered during infection, suggesting that B cell expansion in adipose
261 tissue is both depot and sex specific. In both males and females, we observed expansion of
262 macrophages and granulocytes (**Figure 4C** and **4D**, respectively), consistent with previous
263 studies of gWAT in male mice (Machado et al., 2021). We further observed expansion of
264 dendritic cells in both male and female mice during infection, but this was more pronounced
265 in males (**Figure 4E**). Taken together, this suggests that immune population dynamics in the
266 iWAT are sex specific.

267 Regarding the T cell effector population, we observed an increase in the proportion of
268 $CD3\varepsilon^+$ $TCR\beta^+$ $CD4^+$ T cells in the iWAT of infected mice (**Figure 4F**) and, in particular, we
269 identified an expansion of T effector (Teff) cells ($CD44^+$ and $CD69^+$) (**Figure 4G**). Whilst the
270 frequency of $CD4^+$ T cells increased in both males and females, the iWAT of infected females
271 contained a higher proportion of Teff cells compared with males. The expanded Teff cells
272 displayed an elevated production of interferon gamma (IFNγ; **Figure 4H**), suggesting that
273 some of these cells are polarised towards a T_H1 phenotype. Furthermore, there was a
274 significant expansion of IL-17A-producing Teff cells (**Figure 4I**), indicating that cells are also
275 polarised to a T_H17 phenotype and are a source of IL-17A. In contrast to our hypothesis, we
276 observed a similar expansion of IL-17A-producing Teff cells in both infected males and
277 females. However, we did observe that expression of the IL-17A receptor (*Il17ra*) is

278 significantly elevated in the iWAT of infected male mice, but not females (**Figure 4J**),
279 suggesting that the adipose tissue of males becomes more responsive to IL-17A signalling
280 during infection. Furthermore, IL-17A was elevated in the serum of infected males and female
281 mice, as well as other inflammatory cytokines such as TNFα and IFNγ, compared to naïve
282 controls (**Figure 4K**, **4L** and **4M**, respectively), consistent with previous reports (Magez et al.,
283 1999; Wu et al., 2017). Moreover, we also detected a significant increase in the levels of
284 circulating IFNγ, TNFα, and IL-17A in stage II HAT patients (similarly in both males and
285 females) compared with healthy controls from the Democratic Republic of Congo (**Figure 4N**,
286 **4O**, and **4P**, respectively), suggesting that this feature of infection is conserved between
287 infected mice and humans.

288 **IL-17A/F limits parasitaemia and clinical outcomes in male mice**

289 Our results so far indicate that chronic iWAT infection leads to an expansion of Th17
290 effector T cells in male mice. However, the role of IL-17 on the control of *T. brucei* infection is
291 not understood. To explore this, we used a global *Il17a/f* knockout mouse, which is deficient
292 in both IL-17a and IL-17f (Haas et al., 2012). We monitored parasitaemia in male (**Figure 5A**)
293 and female (**Figure 5B**) *Il17af*$^{-/-}$ mice over the course of infection. We observed that the first
294 peak of parasitaemia was similar between wildtype and *Il17af*$^{-/-}$ male mice, but at late
295 timepoints the *Il17af*$^{-/-}$ males displayed consistent higher levels of parasitaemia than their
296 wildtype counterparts, indicating that IL-17A/F is essential to control infection during the
297 chronic stage of the infection in male mice. In contrast, although not significant, the first peak
298 of parasitaemia in *Il17af*$^{-/-}$ females was lower than in wild type mice, and the second peak of
299 parasitaemia was delayed. Deletion of *Il17a/f* was also associated with an earlier onset and
300 increased severity of clinical symptoms in both males (**Figure 5C**) and females (**Figure 5D**).
301 *Il17af*$^{-/-}$ *m*ale and female mice started to exhibit clinical symptoms (piloerection and hunching)
302 from 3 and 7 dpi, respectively, whereas wild type mice started to experience these symptoms
303 between 12 and 15 dpi. Unlike bloodstream parasite numbers, the parasite burden of the major
304 adipose tissue depots does not appear to be influenced by IL-17A/F in either sex (**Figure 5E**
305 a**nd 5G**). Together, these findings suggest that IL-17A/F play a critical role in controlling

306 parasitaemia during the chronic stages of the infection, and in modulating clinical symptoms
307 in mice infected with *T. brucei*.

308 **IL-17A/F influences bodyweight and feeding behaviour in male mice during infection**

309 Our data so far indicate that chronic *T. brucei* infection leads to an accumulation of
310 T_H17 effector cells in the iWAT, as well as a significant increase of *Il17a* receptor expression,
311 indicating both local IL-17 production and a potential increase in IL-17A receptor signalling.
312 Therefore, we next asked whether IL-17A/F insufficiency leads to weight loss during infection.
313 As previously in this study, we monitored the weight of both male and female mice during the
314 course of infection. Unlike wild type male mice, infected *Il17af* knockout (*Il17af*$^{-/-}$) males
315 maintained their weight until 19 dpi, after which they started to gain significantly more weight
316 than infected wild type males (**Figure 6A**). In contrast, infected female *Il17af*$^{-/-}$ mice started to
317 gain weight in a similar pattern to wild type females, although similarly to males, knockout
318 females gained more weight that their wild type counterparts (**Figure 6B**). Some of this weight
319 gain was related to increased splenomegaly in *Il17af*$^{-/-}$ females, compared with their wild type
320 counterparts (**Supplementary Figure 2A**).

321 It was previously observed that when it is administered to wild type naïve mice, IL-17A
322 suppresses food intake (Nogueira et al., 2020). Therefore, to understand whether IL-17A
323 influences feeding behaviour and drives weight loss during infection, gross food intake was
324 measured for naïve and infected *Il17af*$^{-/-}$ mice. Until 9 dpi, wild type and *Il17af*$^{-/-}$ male mice
325 reduced their food intake at the same rate (**Figure 6C**). However, after 11dpi, *Il17af*$^{-/-}$ mice
326 started to increase their food intake above that of the wild types. Indeed, food intake for
327 infected *Il17af*$^{-/-}$ mice was higher between 15 and 23 dpi compared with at the onset of
328 infection. Unlike male mice, feeding behaviour was indistinguishable between infected female
329 *Il17af*$^{-/-}$ and wild type mice (**Figure 6D**). Together, this may suggest that IL-17A/F regulate
330 bodyweight by potentially suppressing the appetite of male mice during infection, but not
331 female mice. Further supporting this hypothesis, we found that naïve *I17af*$^{-/}$ male mice have
332 significantly higher mass of iWAT than wild type males (**Figure 6E**), and this was not a result
333 of increased splenomegaly in this genotype compared with wild type males (**Supplementary**

334 **Figure 2B**). Upon infection, *Il17af*$^{-/-}$ knockout male mice also retained more of their iWAT mass
335 compared with their wild type counterparts, suggesting that they experienced less wasting. In
336 contrast to this, although naïve *I17af*$^{-/}$ female mice have a higher mass of iWAT than their wild
337 type counterparts, they experience similar levels of wasting as wild type females upon infection
338 (**Figure 6F**), supporting the assertion that the effects of IL-17A/F are sex-dependent.

339 To understand whether deletion of *Il17af*$^{-/-}$ impacts iWAT lipid content, we performed
340 H&E staining on the iWAT (**Figure 6G**) and measured lipid droplet size in naïve and infected
341 male (**Figure 6H**) and female (**Figure 6I**) mice and compared these with wild type animals.
342 The iWAT adipocyte size was indistinguishable between genotypes in naïve animals.
343 However, upon infection, *Il17af*$^{-/-}$ males retained a higher frequency of larger lipid droplets than
344 wild type males (**Figure 6H**). When comparing this to female mice, we found that deletion of
345 *Il17af*$^{-/-}$ had no impact on the range of lipid droplet sizes (**Figure 6I**). This observation indicates
346 that IL-17A/F signalling drives lipid usage in adipocytes in males, but not in females, during
347 infection. We reasoned that the changes in weight, feeding behaviour, and lipid usage may
348 result from IL-17A signalling in the hypothalamus (Aviello et al., 2021), as adipose tissue
349 function and feeding are centrally controlled by this brain structure (Zhang et al., 2014). Using
350 single molecule fluorescence *in situ* hybridisation (smFISH), we observed transcription of
351 *Il17ra*, the gene encoding the IL-17A receptor, in proximity to neurons in the arcuate nucleus
352 of the hypothalamus in both naïve and infected male mice (**Figure 6J**). *Il17ra* expression
353 occurred in proximity to neurons expressing agouti-related neuropeptide (*Agrp*) and pro-
354 melanin concentrating hormone (*Pmch*), which are involved in promotion or suppression of
355 feeding, respectively (Aponte et al., 2011). These observations suggest that the hypothalamus
356 in general, and neurons controlling appetite and feeding behaviour in particular, are primed to
357 sense IL-17 *via Il17ra*. In conjunction with increased levels of circulating IL-17A, we propose
358 that during chronic infection with *T. brucei*, increased circulating levels of IL-17 lead to
359 hypothalamic dysfunctions to suppress feeding, also driving weight loss in male mice.
360
361

362 **Discussion**

363 In this study, we wanted to understand the impact that African trypanosomes have on
364 adipose tissue wasting in the subcutaneous adipose tissue depot, and whether this is
365 mediated by components of the immune system. Throughout this study, we uncovered
366 evidence demonstrating that male mice are more susceptible to trypanosomiasis-induced
367 weight loss and adipose tissue wasting than female mice, and that IL-17A/F plays a key role
368 in this sexually dimorphic pathology. Furthermore, we found that IL-17A/F suppresses food
369 intake in males but not in females, potentially suggesting a dual effect of this cytokine; either
370 locally in adipocytes, or in the hypothalamus to promote changes in feeding behaviour. Indeed,
371 changes in feeding behaviour due to altered hypothalamic signalling may play a key role in
372 the pathology that we observe during infection and may be an indirect consequence of
373 perturbations within the central nervous system. Notably, we also observed elevation of
374 circulating IL-17A in HAT patients, suggesting that this cytokine plays a role in the human
375 immune response to *T. brucei* infection. It is, therefore, tempting to speculate that IL-17A could
376 also play a role in mediating the weight loss experienced by patients infected with *T. brucei*.

377 **Sexual dimorphism in the response to infection with *T. brucei***

378 Previous studies have focused primarily on the use of a single sex during *T. brucei*
379 infection, with a limited number of studies comparing sexes when measuring effects on
380 reproductive organs (Carvalho et al., 2018; Raheem, 2014). It is understood that males and
381 females display multiple differential responses to infection, including differences in sickness
382 behaviour (Vale and Jardine, 2015), weight loss (Cernetich et al., 2006), and the immune
383 response (Klein and Flanagan, 2016). This aligns with the results presented here, where we
384 observe differences in behaviour, weight loss and the immune response between male and
385 female mice during infection. In the study presented here, weight loss in male mice was
386 coupled with decreased iWAT mass. This was associated with a bigger decrease in adipocyte
387 lipid droplet size in male than in female mice, potentially indicating that male mice utilise their
388 lipid stores at a faster rate than females. Alternatively, this may be a result of females
389 preferentially storing lipids in iWAT compared with males (Uranga et al., 2005), and so

390 throughout infection they are able to store more fatty acids obtained from their diet than males,
391 slowing down lipid droplet shrinkage. Due to this loss of lipid content, we hypothesised that
392 circulating glycerol, which is a proxy for measuring adipocyte lipolysis (Jansson et al., 1992),
393 would be elevated during infection. However, we found that in both HAT patients and mice
394 circulating glycerol levels are diminished during trypanosomiasis, supporting the idea that
395 adipocytes become dysfunctional and limit their nutrient release. Decreased circulating
396 glycerol may also occur as a result of adipocyte death, and so there are fewer adipocytes
397 releasing nutrients into circulation. We speculate that since lipolysis is a critical regulator of
398 multiple immune compartments, including macrophages (Kosteli et al., 2010) and $CD4^+$ T cells
399 (Ioan-Facsinay et al., 2013), that downregulation of this pathway will also impair the immune
400 response to infection. Further work is required to elucidate if this also takes places in African
401 trypanosomiasis.

402 To further understand the processes driving the adipocyte shrinkage that we observed
403 in male and female mice during infection, we performed bulk transcriptomic analyses on the
404 iWAT. This supported our findings that adipose tissue lipolysis is diminished during infection,
405 showing extensive downregulation of genes associated with mitochondrial metabolism and
406 lipolysis in both males and females. This suppression of metabolic pathways has been
407 observed in response to infection with other pathogens, such as *Mycobacterium tuberculosis*
408 (Shi et al., 2015). During early *M. tuberculosis* infection of the lungs, transcripts encoding
409 enzymes of oxidative phosphorylation and the tricarboxylic acid cycle are downregulated (Shi
410 et al., 2015). Furthermore, in diseases such as anorexia nervosa, prolonged weight loss and
411 negative energy balance, lipolysis decreases, which is hypothesised to preserve energy that
412 is needed to maintain processes essential to survival (Xiao et al., 2020). In the context of
413 sleeping sickness and nagana, prolonged weight loss may result in the adipose tissue shutting
414 down its main metabolic functions to preserve energy, although we cannot rule out that this
415 downregulation is caused by the loss of adipocytes and, and therefore, underrepresentation
416 of transcripts from these cells.

417 **Sexual dimorphism in the adipose tissue immune response to IL-17A/F during *T. brucei***
418 **infection**

419 Previous studies of adipose tissue immune response focused exclusively on the gWAT
420 of male mice, and identified an expansion of macrophage, Teff cell, and B cell populations
421 (Carvalho et al., 2018). In agreement with this study, we also observed an expansion of
422 macrophages and Teff cells. However, we also noted that there was a reduction in the
423 proportion of B cells in the iWAT of male mice, and no changes in females, suggesting that
424 this is a tissue- and sex-specific response.

425 Our observation that IL-17A signalling may be increased in mice and humans during
426 infection with *T. brucei* led us to question whether this impacts adipose tissue structure and/or
427 function. Genetic ablation of IL-17A and IL-17F prevented weight loss in *T. brucei*-infected
428 male mice, but not in females, which gained weight over the course of infection to a similar
429 rate to their wild type counterparts. This may be due to differences in feeding behaviour
430 throughout the experiment, with *Il17af*$^{-/-}$ males eating more than wild type males, which is
431 centrally regulated in the brain by the hypothalamus. Indeed, we observed an upregulation of
432 *Il17ra* expression in both the iWAT and hypothalamus during chronic infection, and there is
433 evidence to suggest that IL-17A influences food intake and feeding behaviour by acting on the
434 hypothalamus under physiological conditions (Nogueira et al., 2020). The study by Nogueira
435 *et al* (2020) supports our findings, as they also observed that IL-17A suppresses appetite,
436 suggesting that IL-17A could play a central role in controlling sickness-induced anorexia during
437 chronic infection.

438 **IL-17 and adipose-hypothalamic interactions**

439 As well as maintaining their weight, male *Il17af*$^{-/-}$ mice retained more of their adipose
440 tissue and experienced less adipocyte hypotrophy than wild type males during infection. There
441 are several plausible explanations for this. Studies of obesity have found that IL-17-producing
442 mucosal-associated invariant T (MAIT) cells are enriched in the adipose tissue of obese
443 children (Carolan et al., 2015), and may influence insulin signalling (Bergin et al., 2022).
444 Zúñiga et al (2010) found that IL-17 deficient male mice were more insulin sensitive than wild

445 types, which may limit lipolysis due to the anti-lipolytic effects of insulin signalling (Jensen,
446 1995). However, it remains unclear which IL-17 isoform led to this effect. Conversely, human
447 studies suggest that decreased concentrations of circulating IL-17A and IL-17F lead to insulin
448 resistance (Zhou et al., 2020). This disparity may result from knockout of other isoforms of IL-
449 17 in mice, or it may indicate that the role of IL-17 in modulating metabolism is context
450 dependent. Alternatively, it is now appreciated that IL-17-producing gamma-delta (γδ) T cells
451 play a physiological role in control of body temperature and adipose tissue immune
452 homeostasis (Hu et al., 2020). During cold exposure, the frequency of IL-17A-producing γδ T
453 cells in the brown adipose tissue increases and promotes non-shivering thermogenesis,
454 whereby the tissue consumes fuel to generate heat (Kohlgruber et al., 2018). It is tempting to
455 speculate that during early *T. brucei* infection, mice switch on their thermogenic program,
456 which contributes to fever generation (Yoneshiro et al., 2021), and this may contribute to
457 additional consumption of lipids in the adipose tissue. Recent studies identified that agouti-
458 related neuropeptide (AGRP; encoded by *Agrp*)-producing neurons in the hypothalamus,
459 which promote feeding contribute to the activation of adipose tissue thermogenesis, and that
460 this, in turn, can influence bodyweight (Han et al., 2021). Further to this, pro-opiomelanocortin
461 (POMC; encoded by *Pmch*)-positive neurons, which suppress feeding, can also promote
462 thermogenesis (Yao et al., 2017). Differential activation of these neurons, therefore, influence
463 the weight of an organism, and their adipose tissue mass. In the context of infection, IL-17A
464 signalling in the hypothalamus drives POMC expression and, with prolonged exposure, AGRP
465 expression (Nogueira et al., 2020). This temporal response to IL-17A suggests that during *T.*
466 *brucei* infection, at early timepoints there is an increase in the activity of POMC-expressing
467 neurons, leading to suppressed food intake, whilst at later timepoints there may be an increase
468 in the activity of AGRP-expressing neurons. However, further studies are required to
469 determine this.

470 Based on all these observations, we propose a model whereby chronic *T. brucei*
471 infection leads to an increase in circulating IL-17A/F in humans and animals, which might act
472 locally in the adipose tissue, by direct signalling through the IL-17 receptor to promote

473 adipocyte lipolysis, as well as in the hypothalamus to modulate feeding behaviour in a sex-
474 dependent manner. Further work genetically manipulating IL-17 signalling in a cell- and/or
475 tissue-specific manner might provide further mechanistic insights into this process. This study
476 provides insights into the metabolic response of adipose tissue during infection with *T. brucei*
477 and how changes in cellular metabolism influence systemic metabolism. Furthermore, this
478 work highlights the sex-dependent effects of IL-17A/F on the adipose tissue responses to
479 infection. Future work is needed to determine the pathways underpinning these sex
480 differences, as well as the potential sources of IL-17A/F during infection, which has
481 implications for sexually dimorphic responses to infectious diseases in humans.
482
483
484
485
486
487
488
489
490
491
492
493
494
495
496
497
498
499
500

501 **Figure Legends**

502 **Figure 1. Male mice lose weight during infection with *Trypanosoma brucei*, which is**
503 **associated with alterations in feeding behaviour. (A)** Number of parasites per mL of blood,
504 measured using phase microscopy and the rapid "matching" method (Herbert and Lumsden,
505 1976). **(B)** Clinical scores of infected male and female mice. **(C)** Percentage changes in body
506 weight of male and **(D)** female mice over the course of infection. Percentage changes in food
507 intake in male **(E)** and female **(F)** mice. Each data point represents 2 cages (*n*=3-4 mice per
508 cage). Time series data were analysed using two-way repeated measures ANOVA with Sidak
509 post-hoc testing and are expressed as mean ±SD. *p<0.05, **p<0.01, ***p<0.001, ns = non-
510 significant.

511

512 **Figure 2. *Trypanosoma brucei* infection leads to reductions in iWAT mass and lipid**
513 **content, as well as impairment of adipose tissue function. (A)** Schematic highlighting the
514 anatomical location of the inguinal white adipose tissue (iWAT). **(B)** Histological analysis of
515 the iWAT and gWAT trypanosome colonisation, using HSP70 staining**. (C)** Parasite burden of
516 iWAT and gWAT**.** Parasite density in the iWAT, which was measured by RT-qPCR of genomic
517 DNA. A comparison was made with gonadal white adipose tissue (gWAT), to understand if
518 the iWAT is also highly colonised. **(D)** iWAT mass at 25 days post-infection or in naïve mice.
519 iWAT was dissected and weighed before normalising to body weight, to account for variation
520 between biological replicates. Symbols indicate the number of biological replicates collected
521 from two independent experiments **(E)** Representative histological H&E staining of iWAT
522 showing adipocyte lipid droplets and immune infiltrate. Magnification = 20X. Insets highlight
523 likely immune cell infiltrate. **(F)** Analysis of lipid droplet area (μm^2) in naïve and infected males
524 and **(G)** females. *N*=6 biological replicates per group, from two independent experiments. Lipid
525 droplets were measured from 3 distinct areas in each image and then combined for each
526 biological replicate. **(H)** Circulating glycerol concentration in naïve vs. infected male and
527 female mice. *n*=4 biological replicates per group. **(I)** Circulating glycerol concentration in
528 healthy vs. infected patients. *N*=5 patients per group and each group is a mix of male and

529 female. For **C**, **D, H** and **I**, data were analysed using a two-tailed Student t test. For **F** and **G**,
530 data were analysed using a two-way ANOVA with Sidak post-hoc testing. Data for all panels
531 are expressed as mean ±SD. *p<0.05, **p<0.01, ***p<0.001, ****p<0.0001, ns = non-
532 significant.
533
534 **Figure 3. Transcriptomic analysis suggests a stronger T cell response in the iWAT of**
535 **males than females. (A)** Principal component analysis of bulk transcriptomic data from male
536 and female naïve and infected mice. **(B)** Venn diagram of genes that were upregulated in
537 infected male and female mice compared with naïve controls, highlighting the number of
538 overlapping or non-overlapping genes. **(C)** Heatmap of the 25 most significantly dysregulated
539 genes during infection. Both naïve and infected groups contain an even number of males and
540 females. **(D)** Heatmap of T_H17 transcripts in male mice. n=4 biological replicates per group.
541
542 **Figure 4. Elevated circulating IL-17A is associated with increased IL-17 receptor A (IL-**
543 **17RA) in male mice during *T. brucei* infection. (A)** Measurements of the proportions of B
544 cells, **(B)** macrophages, **(C)** granulocytes, and **(D)** dendritic cells. **(E)** Representative viSNE
545 plots highlighting the gating strategy for analysis of $CD4^+$ cells. We gated on CD45+, CD3ε,
546 TCRβ, CD4+ cells. **(F)** Measurements of the proportions of $CD4^+$, **(G)** T effector (Teff), **(H)**
547 IFNγ-producing and **(I)** IL-17A-producing T cells. **(J)** Expression of interleukin-17A receptor
548 (*Il17ra*) mRNA in infected male and female mice. Measurements of circulating serum IL-17A,
549 TNFa, and IFNγ in mice **(K**, **L**, **M)** and IFNγ, TNFa and total IL-17 in humans **(N**, **O**, **P)**. Mouse
550 cytokine data were collected from samples taken across three independent experiments. Data
551 were tested for normal distribution and analysed by either one-way ANOVA or a Kruskal Wallis
552 test. Biological replicates are indicated by symbols for each panel. Data points indicate
553 biological replicates for each panel. Data for all panels are expressed as mean ±SD. *p<0.05,
554 **p<0.01, ***p<0.001, ****p<0.0001, ns = non-significant.

555 **Figure 5. IL-17A/F limits parasitaemia and clinical symptoms during *T. brucei* infection.**
556 Number of parasites per mL of blood in *Il17af*$^{-/-}$ vs wild type male **(A)** and female **(B)** mice,
557 which was measured using phase microscopy and the rapid "matching" method (Herbert and
558 Lumsden, 1976). **(C** and **D)** Parasite burden of iWAT and gWAT. **(E** and **F)** Clinical scores of
559 infected male and female mice. iWAT = inguinal white adipose tissue; gWAT = gonadal white
560 adipose tissue; BAT = brown adipose tissue. Symbols indicate the number of biological
561 replicates per group. Data are expressed as mean ±SD. *p<0.05, **p<0.01, ns = non-
562 significant.
563
564 **Figure 6. Deletion of *Il17a* and *Il17f* limits weight loss and adipose tissue wasting, and**
565 **alters feeding behaviour in males infected with *Trypanosoma brucei*. (A)** Percentage
566 changes in bodyweight of wild type and *Il17af*$^{-/-}$ male mice over the course of infection. n=7
567 mice per group across two independent experiments. **(B)** Percentage weight changes in
568 bodyweight of wild type and *Il17af-/-* female mice over the course of infection. **(C and D**)
569 Changes in gross food intake over the course of infection. Each data point represents 2 cages
570 (n=3-4 mice per condition) from 2 independent experiments. **(E)** iWAT mass in naïve wild type
571 and *Il17af-/-* male mice. **(F)** iWAT mass in naïve wild type and *Il17af-/-* female mice. **(G)** H&E
572 staining of iWAT from male and female *Il17af*$^{-/-}$ mice. Analysis of lipid droplet area (μm^2) in
573 naïve and infected males **(H)** and **(I)**. Lipid droplets were measured from 3 distinct areas in
574 each image and then combined for each biological replicate. **(J)** Single molecule fluorescence
575 *in situ* hybridisation imaging of the hypothalamus from naïve and infected male C57BL/6 mice.
576 IIIV = 3rd ventricle; β1 and β2 = tanycytes; ARH = arcuate nucleus of the hypothalamus; *Agrp*
577 = agouti-related neuropeptide; *Pmch* = pro-melanin concentrating hormone; *Il17ra* = IL-17A
578 receptor. Data for wild type mice in panels **A, B, C**, and **D** are taken from Figure 1. Data for
579 wild type mice in panels **E, F, G,** and **H** are taken from Figure 3. Data in panels **A, B, C,** and
580 **D** were analysed using two-way repeated measures ANOVA with Sidak post-hoc testing. Data
581 in panels **E** and **F** were analysed using one-way ANOVA with Tukey post-hoc testing. Data
582 points represent biological replicates. Data in panels **A** – **I** are from 2-3 independent

583 experiments. Data are expressed as ±SD. **p<0.01, ***p<0.001, ****p<0.0001, ns = non-
584 significant
585
586 **Supplementary Figure Legends**
587 **Supplementary Figure 1, related to Figure 2. Spleen mass increases in both male and**
588 **female mice during infection.** Spleen weights were normalised to bodyweight and the fold
589 change in weight calculated. Each point represents a biological replicate. Data were analysed
590 using one-way ANOVA with Tukey post-hoc testing. ****p<0.0001.
591
592 **Supplementary Figure 2, related to Figure 6. Spleen mass is higher in *Il17af*$^{-/-}$ than wt**
593 **females during infection.** Spleen weights from males **(A)** and females **(B)** were normalised
594 to bodyweight and the fold change in weight calculated. Each point represents a biological
595 replicate. Data were analysed using one-way ANOVA with Tukey post-hoc testing.
596 ****p<0.0001.
597
598
599
600
601
602
603
604
605
606
607
608
609
610

611 **Materials & Methods**

612 **Ethics statement**

613 Human serum samples used for glycerol measurements were collected in Guinea as
614 part of the National Control Program. Participants were informed of the study objectives in
615 their own language and signed a written consent form. Human serum samples used for IL-
616 17A measurements were collected as part of the TrypanoGEN Biobank, with ethical approval
617 from the Democratic Republic of Congo National Ministry of Public Health (approval number
618 1/2013). Samples were used from different regions due to limitations in sample availability.
619 Ethical approval to use all human samples outlined in this study was given by the University
620 of Glasgow (Project No: 200120043). All animal experiments were approved by the University
621 of Glasgow Ethical Review Committee and performed in accordance with the home office
622 guidelines, UK Animals (Scientific Procedures) Act, 1986 and EU directive 2010/63/EU. All
623 experiments were conducted under SAPO regulations and UK Home Office project licence
624 number PC8C3B25C to Dr Jean Rodgers.

625 **Murine infections with *Trypanosoma brucei***

626 Six to eight weeks old male or female C57Black/6Jm (JAX, stock 000664) or *Il17af*$^{-/-}$
627 (stock 034140, The Jackson Laboratory, Maine, USA) mice were inoculated by intra-peritoneal
628 injection with ~2 x 10^3 parasites of strain *T. brucei brucei* Antat 1.1^E (Le Ray et al., 1977).
629 Parasitaemia was monitored by regular sampling from tail venesection and examined using
630 phase microscopy and the rapid "matching" method (Herbert and Lumsden, 1976). Uninfected
631 mice of the same strain, sex and age served as uninfected controls. All mice were fed *ad*
632 *libitum* and kept on a 12 h light–dark cycle. All *in vivo* experiments were concluded at 25 days
633 post-infection, to model chronic infection in humans.

634 **RNA Purification**

635 iWAT was harvested from mice and stored in TRIzol™ (Cat. #15596026, Invitrogen,
636 Massachusetts, USA). Total RNA was then purified from iWAT using an RNeasy Kit (Cat.
637 #74004, Qiagen, Dusseldorf, Germany) as per the manufacturer's recommendations. The
638 RNA was purified in 30 µL of nuclease-free water (Cat. #129112, Qiagen, Dusseldorf,

639 Germany), and RNA concentration measured on a NanoDrop™ 2000 (Cat. #ND2000, Thermo
640 Fisher Scientific, Massachusetts, USA). Samples were shipped to Novogene (Cambridge, UK)
641 to undergo quality control, library preparation and sequencing. RNA integrity was assessed
642 using an RNA Nano 6000 Assay Kit (Cat. # 5067-1511, Agilent Technologies, California, USA)
643 with a Bioanalyzer 2100 (Agilent Technologies, California, USA), as per the manufacturer's
644 instructions. Samples with an RNA integrity number (RIN) of >6.0 were qualified for RNA
645 sequencing.

646 **Library Preparation**

647 Library preparation was performed by Novogene (Cambridge, UK). Messenger RNA
648 (mRNA) was purified from total RNA using poly-T oligo-attached magnetic beads.
649 Fragmentation was carried out using divalent cations under elevated temperature in a First
650 Strand Synthesis Reaction Buffer (5X). First strand cDNA was synthesized using random
651 hexamer primers and M-MuLV Reverse Transcriptase (RNase H-). Second strand cDNA
652 synthesis was then performed using DNA Polymerase I and RNase H. Remaining overhangs
653 were converted to blunt ends *via* exonuclease/polymerase activity. Following adenylation of
654 3' ends of DNA fragments, adaptors with hairpin loop structures were ligated. To select cDNA
655 fragments of 370~420 bp in length, library fragments were purified using AMPure XP beads
656 (Beckman Coulter, Beverly, USA), as per the manufacturer's instructions. PCR was then
657 performed using Phusion High-Fidelity DNA polymerase, Universal PCR primers, and Index
658 (X) primers. Finally, PCR products were purified (AMPure XP system) using AMPure XP
659 beads (Beckman Coulter, Beverly, USA), as per the manufacturer's instructions, and library
660 quality was assessed using a Bioanalyzer 2100 (Agilent Technologies, CA, USA).

661 **Sequencing and data analysis**

662 Clustering of the index-coded samples was performed on a cBot Cluster Generation
663 System using a TruSeq PE Cluster Kit v3-cBot-HS (Illumia, California, USA) according to the
664 manufacturer's instructions. After cluster generation, libraries were sequenced on an Illumina
665 Novaseq platform and 150 bp paired-end reads were generated. Raw reads in fastq format
666 were processed through proprietary Perl scripts developed by Novogene (Cambridge, UK).

667 Clean reads were obtained by removing reads containing adapters, poly-N, or low-quality
668 reads from raw data. Concurrently, the Q20, Q30 and GC content of the clean data was
669 calculated. Genome and genome annotation files (Genome Reference Consortium Mouse
670 Build; GRCm39) were downloaded. An index of the reference genome was built using Hisat2
671 v2.0.5 and paired-end clean reads were aligned to the reference genome using Hisat2 v2.0.5.
672 The featureCounts (v. 1.5.0-p3) package was used to count read numbers mapped to each
673 gene, before calculating the Fragments Per Kilobase of transcript sequence per Millions base
674 pairs (FPKM) of each gene using the length of the gene and reads count mapped to this gene.
675 Differential expression analysis was performed using the DESeq2 R package (v. 1.20.0).
676 DESeq2 The resulting *p*-values were adjusted using the Benjamini and Hochberg approach
677 to control false discovery rate. Genes with an adjusted *p*-value of <0.05 were assigned as
678 differentially expressed. Pathway enrichment analysis of differentially expressed genes was
679 performed using the ShinyGO (v. 0.76) package (Ge et al., 2020), mapping genes to the Kyoto
680 Encyclopaedia of of Genes and Genomes (KEGG) database (Kanehisa et al., 2021). KEGG
681 terms with an adjusted *p*-value <0.05 were considered significantly enriched. Heatmaps were
682 generated using the pheatmap (Version 1.0.12) and Tidyverse (Wickham et al., 2019)
683 packages in R (Version 4.2.1). Samples were clustered by Euclidean distance.

684 **DNA Purification**

685 Tissues were harvested from mice and snap frozen. Tissue was digested using a
686 DNeasy Blood and Tissue kit (Cat. #69504, Qiagen, Dusseldorf, Germany), before purifying
687 DNA as per the manufacturer's instructions. DNA was eluted in 100 µL of EB buffer (Cat. #
688 19086, Qiagen, Dusseldorf, Germany).

689 **Tissue Parasite Burden Quantification**

690 To quantify *T. brucei* parasites in tissue, we amplified 18S ribosomal DNA genes from
691 the gDNA of a known mass of tissue, using qRT-PCR Brilliant II Probe Master Mix (Cat.
692 #600809, Agilent Technologies, California, USA) with a TaqMan™ TAMRA Probe system
693 (Cat. #450025, Applied Biosystems, Massachusetts, USA). Primer sequences were specific
694 to *T. brucei* 18S ribosomal DNA (**Table 1**). The cycling conditions used for qRT-PCR are

695 outlined in **Table 2**. Generated data was converted to parasite copy number using a standard
696 curve.

Primer/probe name	Primer/probe sequence
TBPFR Forward Taqman primer	CCA ACC GTG TGT TTC CTC CT
TBPFR Reverse Taqman primer	CGG CAG TAG TTT GAC ACC TTT TC
TBPFR probe	5'-FAM CTT GTC TTC TCC TTT TTT GTC TCT TTC CCC CT 3'TAMRA

697 **Table 1.** Primer and probe sequences for tissue parasite burden quantification

Step	Temperature	Time	Number of cycles
1	95	10 minutes	1
2	95	15 seconds	45
3	60	1 minutes	
4	72	1 seconds	

698 **Table 2.** Thermal cycling conditions for tissue parasite burden quantification

699 **Histological Analyses**

700 Tissues were placed into 4% paraformaldehyde (PFA) and fixed overnight at room
701 temperature. PFA-fixed tissues were then embedded in paraffin, sectioned, and stained by
702 the Veterinary Diagnostic Services facility (University of Glasgow, UK). Sections were
703 Haematoxylin and Eosin (H&E) stained for lipid droplet measurement analysis, or 3'-
704 diaminobenzidine (DAB) stained for heat-shock protein 70 (HSP70) to detect *T. brucei*
705 parasites. The HSP70 antibody was a kind gift from Professor James D. Bangs. Slide imaging
706 was performed by the Veterinary Diagnostic Services facility (University of Glasgow, UK) using
707 an EasyScan Infinity slide scanner (Motic, Hong Kong) at 20X magnification. To determine
708 lipid droplet sizes in adipose tissue, images were first opened in QuPath (v. 0.3.2) (Bankhead
709 et al., 2017), before selecting regions and exporting to Fiji (Schindelin et al., 2012). In Fiji,

710 images were converted to 16-bit format, and we used the Adiposoft plugin to quantify lipid
711 droplet area within different sections.

712 **Immunofluorescence and single molecule fluorescence *in situ* hybridisation (smFISH)**
713 **using RNAscope**

714 To prepare tissue sections for smFISH, infected animals and naïve controls were
715 anesthetized with isoflurane, brains were dissected out into 4% PFA. Following overnight
716 fixation in 4% PFA, tissues were embedded in paraffin, and sectioned by the Veterinary
717 Diagnostic Services facility (University of Glasgow, Glasgow, UK). An RNAscope 2.5 Assay
718 (Advanced Cell Diagnostics, California, USA) was used for all smFISH experiments, according
719 to the manufacturer's protocols. All RNAscope smFISH probes (**Table 3**) were designed and
720 validated by Advanced Cell Diagnostics. For image acquisition, 16-bit laser scanned confocal
721 images were acquired using the 63x/1.4 plan-apochromat objective of an LSM 880 confocal
722 microscope (Zeiss, Oberkochen, Germany). smFISH images were acquired with minor
723 contrast adjustments as needed, and converted to grayscale, to maintain image consistency.
724 The resulting images were processed and analysed using Fiji (Schindelin et al., 2012), and
725 the values plotted using GraphPad Prism (v. 8.0).

List of RNAScope probes used for smFISH			
***Mus musculus* probes**			
Supplier	**Catalogue number**	**Sequence**	**Channel**
Biotechne	403741	Mm-*Il17ra*	Channel 1
Biotechne	478728-C2	Mm-*Pmch*	Channel 2
Biotechne	400711-C4	Mm-*Agrp*	Channel 4

726 **Table 3** smFISH probes used for RNAScope

727 **Mass cytometry sample processing**

728 Adipose tissue was dissected out and transferred to PBS, before dissociating using an
729 Adipose Tissue Dissociation Kit for Mouse and Rat (Cat. # 130-105-808, Miltenyi Biotec,
730 Cologne, Germany), using a gentleMACS™ Octo Dissociator with Heaters (Cat. #130-096-

731 427, Miltenyi Biotec, Cologne, Germany), as per the manufacturer's recommendations. After
732 the final recommended centrifugation, the pellet (containing the immune cells) was
733 resuspended in Dubecco's Modified Eagle Medium (DMEM) to a concentration of 1 x 10^6
734 cells/mL. Cells were activated for 6 h in a round-bottom 96-well plate using Cell Activation
735 Cocktail (with Brefeldin A) (Cat. #423304, BioLegend, San Diego, USA) as per the
736 manufacturer's recommendations. Plates were then centrifuged at 300 x g for 5 min and the
737 pellets resuspended in 50 µL of Cell-ID™ Cisplatin-195Pt viability reagent (Cat. # 201195,
738 Standard BioTools, San Francisco, USA), and incubated at room temperature for 2 min. Cells
739 were washed twice in Maxpar® Cell Staining Buffer (Cat. # 201068, Standard BioTools, San
740 Francisco, USA), and centrifuged at 300 x g at room temperature for 5 min. The CD16/CD32
741 receptors were then blocked by incubating with a 1/50 dilution of TruStain FcX™ (Cat.
742 #101319, BioLegend, San Diego, USA) in PBS at room temperature for 15 min. An antibody
743 cocktail was prepared (**Table 4**) from the Maxpar® Mouse Sp/LN Phenotyping Panel Kit (Cat.
744 #201306, Standard BioTools, San Francisco, USA), with additional antibodies against IL-17A,
745 IFNγ, TCRgd, and CD27 included (**Table 4**). Cells were incubated with antibodies (**Table 4**)
746 for 60 min, on ice before washing 3 times in Maxpar® Cell Staining Buffer (Cat. # 201068,
747 Standard BioTools, San Francisco, USA) as previously.
748 Following staining, cells were fixed in 2% paraformaldehyde (PFA) overnight at 4°C.
749 Cells were then washed twice with 1 x eBioscience™ Permeabilization Buffer (Cat. #00-8333-
750 56, Invitrogen, Waltham, USA) at 800 x g at room temperature for 5 min. The pellets were
751 resuspended in intracellular antibody cocktail (**Table 4**) and incubated at room temperature
752 for 45 min. Cells were washed 3 times in Maxpar® Cell Staining Buffer (Cat. # 201068,
753 Standard BioTools, San Francisco, USA) at 800 x g. The cells were then resuspended in 4%
754 PFA at room temperature for 15 min, before collecting the cells at 800 x g and resuspending
755 in Cell-ID™ Intercalator-Ir (Cat. # 201192A, Standard BioTools, San Francisco, USA). Finally,
756 the cells were barcoded by transferring the stained cells to a fresh tube containing 2 µL of
757 palladium barcode from the Cell-ID™ 20-Plex Pd Barcoding Kit (Cat. # 201060, Standard

758 BioTools, San Francisco, USA). Cells were then frozen in a freezing solution (90% FBS and
759 10% DMSO), before shipping to the Flow Cytometry Core Facility at the University of
760 Manchester for data acquisition.

Surface Antibodies				
Antibody	**Metal Conjugate**	**Clone**	**Concentration**	**Cat. No.**
Ly6G/C [Gr1]	141Pr	RB6-8C5	1/100	201306
CD11c	142Nd	N418	1/100	
CD69	145Nd	H1.2F3	1/100	
CD45	147Sm	30-F11	1/200	
CD11b	148Nd	M1/70	1/100	
CD19	149Sm	6D5	1/100	
CD3e	152Sm	145-2C11	1/100	
TCRβ	169Tm	H57-597	1/100	
CD44	171Yb	IM7	1/100	
CD4	172Yb	RM4-5	1/100	
Intracellular Antibodies				
IL-17A	174Yb	TC11-18H10.1	1/100	3174002C
IFNγ	165Ho	XMG1.2	1/100	3165003B

761 **Table 4** Antibodies for mass cytometry

762 **Quantification of cytokine titres**

763 To measure cytokine titres in murine serum samples we used a U-PLEX Biomarker kit
764 (Meso Scale Discovery, Rockville, USA), as per the manufacturer's instructions. Samples
765 were analysed using a MESO QuickPlex SQ 120 (Meso Scale Discovery, Rockville, USA). IL-
766 17A titres in human serum samples were quantified using a multiplex cytokine panel
767 (M500KCAF0Y; Bio-Plex Pro Human Cytokine Assay (BioRad) and a LuminexCorp Luminex
768 100 machine as per the manufacturer's instructions.

769 **Statistical analyses**

770 All statistical analyses were performed using Graph Prism Version 8.0 for Windows or
771 macOS, GraphPad Software (La Jolla California USA). Normality of data distribution was
772 measured using the Shapiro-Wilks test. Where indicated, data were analysed by unpaired
773 Student's t-test, Mann-Whitney test, one-way analysis of variance (ANOVA) or two-way
774 ANOVA. Data were considered to be significant where $p < 0.05$.

775 **Data Availability**

776 The GEO accession number for transcriptomic sequencing data reported in this paper
777 is: GSE21060.

778 **Acknowledgements**

779 We firstly thank the TrypanoGEN Network for providing serum samples from patients.
780 We also thank Jean Rodgers for the use of her project licence for performing animal work. We
781 thank the Histology Research Service at Veterinary Diagnostic Services, School of Veterinary
782 Medicine, University of Glasgow. We also thank Nicola Munro, Scott McCall and Catrina Boyd
783 at the Veterinary Research Facility (University of Glasgow) for maintaining optimal husbandry
784 conditions and comfort for the animals used in this study. Finally, the authors would like to
785 thank the Flow Cytometry Core Facility, University of Manchester, UK, for mass cytometry
786 sample acquisition. This work was funded in part by a Wellcome Trust Institutional Strategic
787 Support Fund and Society for Endocrinology Early Career Grant to MCS. This work was also
788 funded in part by a Wellcome Trust Senior Research Fellowship [209511/Z/17/Z] awarded to
789 AML. JFQ is funded by a Sir Henry Wellcome postdoctoral fellowship (221640/Z/20/Z to JFQ).
790 PC is funded by Wellcome Centre for Integrative Parasitology FutureScope grant to JFQ
791 [310358-01]. GPW is funded by an MRC grant (MR/S009779/1). CB is funded by an MRC
792 grant [MR/W018497/1]. SK is funded by the National Institute of Diabetes and Digestive and
793 Kidney Diseases and the Howard Hughes Medical Institute. The authors declare that the
794 research was conducted in the absence of any commercial or financial relationships that could
795 be construed as a potential conflict of interest.

796

Bibliography

Adelman JS, Martin LB. 2009. Vertebrate sickness behaviors: Adaptive and integrated neuroendocrine immune responses. *Integr Comp Biol* **49**:202–214. doi:10.1093/ICB/ICP028

Aponte Y, Atasoy D, Sternson SM. 2011. AGRP neurons are sufficient to orchestrate feeding behavior rapidly and without training. *Nat Neurosci* **14**:351. doi:10.1038/NN.2739

Aviello G, Cristiano C, Luckman SM, D'Agostino G. 2021. Brain control of appetite during sickness. *Br J Pharmacol* **178**:2096–2110. doi:10.1111/BPH.15189

Baazim H, Antonio-Herrera L, Bergthaler A. 2022. The interplay of immunology and cachexia in infection and cancer. *Nat Rev Immunol* **22**:309–321. doi:10.1038/S41577-021-00624-W

Bankhead P, Loughrey MB, Fernández JA, Dombrowski Y, McArt DG, Dunne PD, McQuaid S, Gray RT, Murray LJ, Coleman HG, James JA, Salto-Tellez M, Hamilton PW. 2017. QuPath: Open source software for digital pathology image analysis. *Scientific Reports 2017 7:1* **7**:1–7. doi:10.1038/s41598-017-17204-5

Bergin R, Kinlen D, Kedia-Mehta N, Hayes E, Cassidy FC, Cody D, O'Shea D, Hogan AE. 2022. Mucosal-associated invariant T cells are associated with insulin resistance in childhood obesity, and disrupt insulin signalling via IL-17. *Diabetologia* **65**:1012–1017. doi:10.1007/S00125-022-05682-W/FIGURES/2

Bukachi SA, Wandibba S, Nyamongo IK. 2017. The socio-economic burden of human African trypanosomiasis and the coping strategies of households in the South Western Kenya foci. *PLoS Negl Trop Dis* **11**. doi:10.1371/JOURNAL.PNTD.0006002

Cabalén ME, Cabral MF, Sanmarco LM, Andrada MC, Onofrio LI, Ponce NE, Aoki MP, Gea S, Cano RC. 2016. Chronic Trypanosoma cruzi infection potentiates adipose tissue macrophage polarization toward an anti-inflammatory M2 phenotype and contributes to diabetes progression in a diet-induced obesity model. *Oncotarget* **7**:13400. doi:10.18632/ONCOTARGET.7630

Capewell P, Cren-Travaillé C, Marchesi F, Johnston P, Clucas C, Benson RA, Gorman TA, Calvo-Alvarez E, Crouzols A, Jouvion G, Jamonneau V, Weir W, Lynn Stevenson M, O'Neill K, Cooper A, Swar NRK, Bucheton B, Ngoyi DM, Garside P, Rotureau B, MacLeod A. 2016. The skin is a significant but overlooked anatomical reservoir for vector-borne African trypanosomes. *Elife* **5**. doi:10.7554/eLife.17716

Carolan E, Tobin LM, Mangan BA, Corrigan M, Gaoatswe G, Byrne G, Geoghegan J, Cody D, O'Connell J, Winter DC, Doherty DG, Lynch L, O'Shea D, Hogan AE. 2015. Altered distribution and increased IL-17 production by mucosal-associated invariant T cells in adult and childhood obesity. *J Immunol* **194**:5775–5780. doi:10.4049/JIMMUNOL.1402945

Carvalho T, Trindade S, Pimenta S, Santos AB, Rijo-Ferreira F, Figueiredo LM. 2018. Trypanosoma brucei triggers a marked immune response in male reproductive organs. *PLoS Negl Trop Dis* **12**. doi:10.1371/JOURNAL.PNTD.0006690

Cernetich A, Garver LS, Jedlicka AE, Klein PW, Kumar N, Scott AL, Klein SL. 2006. Involvement of gonadal steroids and gamma interferon in sex differences in response to blood-stage malaria infection. *Infect Immun* **74**:3190–3203. doi:10.1128/IAI.00008-06/SUPPL_FILE/TABLE_S3.DOC

Childs CE, Calder PC, Miles EA. 2019. Diet and Immune Function. *Nutrients* **11**. doi:10.3390/NU11081933

Choe SS, Huh JY, Hwang IJ, Kim JI, Kim JB. 2016. Adipose tissue remodeling: Its role in energy metabolism and metabolic disorders. *Front Endocrinol (Lausanne)* **7**:30. doi:10.3389/FENDO.2016.00030/BIBTEX

Chusyd DE, Wang D, Huffman DM, Nagy TR. 2016. Relationships between Rodent White Adipose Fat Pads and Human White Adipose Fat Depots. *Front Nutr* **3**:1. doi:10.3389/FNUT.2016.00010

Dahlman I, Mejhert N, Linder K, Agustsson T, Mutch DM, Kulyte A, Isaksson B, Permert J, Petrovic N, Nedergaard J, Sjölin E, Brodin D, Clement K, Dahlman-Wright K, Rydén M,

Arner P. 2010. Adipose tissue pathways involved in weight loss of cancer cachexia. *Br J Cancer* **102**:1541. doi:10.1038/SJ.BJC.6605665

Duncan RE, Ahmadian M, Jaworski K, Sarkadi-Nagy E, Sul HS. 2007. Regulation of Lipolysis in Adipocytes. *Annu Rev Nutr* **27**:79. doi:10.1146/ANNUREV.NUTR.27.061406.093734

Finn PF, Dice JF. 2006. Proteolytic and lipolytic responses to starvation. *Nutrition* **22**:830–844. doi:10.1016/J.NUT.2006.04.008

Galarraga M, Campión J, Munõz-Barrutia A, Boqué N, Moreno H, Martínez JA, Milagro F, Ortiz-de-Solórzano C. 2012. Adiposoft: automated software for the analysis of white adipose tissue cellularity in histological sections. *J Lipid Res* **53**:2791–2796. doi:10.1194/JLR.D023788

Ge SX, Jung D, Jung D, Yao R. 2020. ShinyGO: a graphical gene-set enrichment tool for animals and plants. *Bioinformatics* **36**:2628–2629. doi:10.1093/BIOINFORMATICS/BTZ931

Guedes PMDM, Gutierrez FRS, Maia FL, Milanezi CM, Silva GK, Pavanelli WR, Silva JS. 2010. IL-17 Produced during Trypanosoma cruzi Infection Plays a Central Role in Regulating Parasite-Induced Myocarditis. *PLoS Negl Trop Dis* **4**. doi:10.1371/JOURNAL.PNTD.0000604

Haas JD, Ravens S, Düber S, Sandrock I, Oberdörfer L, Kashani E, Chennupati V, Föhse L, Naumann R, Weiss S, Krueger A, Förster R, Prinz I. 2012. Development of Interleukin-17-Producing γδ T Cells Is Restricted to a Functional Embryonic Wave. *Immunity* **37**:48–59. doi:10.1016/j.immuni.2012.06.003

Han Y, Xia G, Srisai D, Meng F, He Yanlin, Ran Y, He Yang, Farias M, Hoang G, Tóth I, Dietrich MO, Chen MH, Xu Y, Wu Q. 2021. Deciphering an AgRP-serotoninergic neural circuit in distinct control of energy metabolism from feeding. *Nature Communications 2021 12:1* **12**:1–16. doi:10.1038/s41467-021-23846-x

Herbert WJ, Lumsden WHR. 1976. Trypanosoma brucei: A rapid “matching” method for estimating the host’s parasitemia. *Exp Parasitol* **40**:427–431. doi:10.1016/0014-4894(76)90110-7

Hu B, Jin C, Zeng X, Resch JM, Jedrychowski MP, Yang Z, Desai BN, Banks AS, Lowell BB, Mathis D, Spiegelman BM. 2020. γδ T cells and adipocyte IL-17RC control fat innervation and thermogenesis. *Nature 2020 578:7796* **578**:610–614. doi:10.1038/s41586-020-2028-z

Hube F, Hauner H. 1999. The role of TNF-alpha in human adipose tissue: prevention of weight gain at the expense of insulin resistance? *Horm Metab Res* **31**:626–631. doi:10.1055/S-2007-978810

Ioan-Facsinay A, Kwekkeboom JC, Westhoff S, Giera M, Rombouts Y, van Harmelen V, Huizinga TWJ, Deelder A, Kloppenburg M, Toes REM. 2013. Adipocyte-derived lipids modulate CD4+ T-cell function. *Eur J Immunol* **43**:1578–1587. doi:10.1002/EJI.201243096

Jansson PA, Larsson A, Smith U, Lönnroth P. 1992. Glycerol production in subcutaneous adipose tissue in lean and obese humans. *J Clin Invest* **89**:1610–1617. doi:10.1172/JCI115756

Jensen MD. 1995. Gender differences in regional fatty acid metabolism before and after meal ingestion. *J Clin Invest* **96**:2297–2303. doi:10.1172/JCI118285

Kanehisa M, Furumichi M, Sato Y, Ishiguro-Watanabe M, Tanabe M. 2021. KEGG: integrating viruses and cellular organisms. *Nucleic Acids Res* **49**:D545–D551. doi:10.1093/NAR/GKAA970

Kennedy PGE. 2019. Update on human African trypanosomiasis (sleeping sickness). *J Neurol* **266**:2334–2337. doi:10.1007/S00415-019-09425-7

Kennedy PGE. 2013. Clinical features, diagnosis, and treatment of human African trypanosomiasis (sleeping sickness). *Lancet Neurol* **12**:186–194. doi:10.1016/S1474-4422(12)70296-X

Klein SL, Flanagan KL. 2016. Sex differences in immune responses. *Nature Reviews Immunology 2016 16:10* **16**:626–638. doi:10.1038/nri.2016.90

906 Kohlgruber AC, Gal-Oz ST, Lamarche NM, Shimazaki M, Duquette D, Nguyen HN, Mina AI,
907 Paras T, Tavakkoli A, von Andrian U, Banks AS, Shay T, Brenner MB, Lynch L. 2018.
908 γδ T cells producing interleukin-17A regulate adipose regulatory T cell homeostasis and
909 thermogenesis. *Nature Immunology 2018 19:5* **19**:464–474. doi:10.1038/s41590-018-
910 0094-2
911 Kosteli A, Sugaru E, Haemmerle G, Martin JF, Lei J, Zechner R, Ferrante AW. 2010. Weight
912 loss and lipolysis promote a dynamic immune response in murine adipose tissue. *J Clin*
913 *Invest* **120**:3466–3479. doi:10.1172/JCI42845
914 Le Ray D, Barry JD, Easton C, Vickerman K. 1977. First tsetse fly transmission of the
915 "AnTat" seroderme of Trypanosoma brucei. *Ann Soc Belg Med Trop* **57**.
916 Machado H, Bizarra-Rebelo T, Costa-Sequeira M, Trindade S, Carvalho T, Rijo-Ferreira F,
917 Pacheco BR, Serre K, Figueiredo LM. 2021. Trypanosoma brucei triggers a broad
918 immune response in the adipose tissue. *PLoS Pathog* **17**:e1009933.
919 doi:10.1371/JOURNAL.PPAT.1009933
920 Magez S, Radwanska M, Beschin A, Sekikawa K, de Baetselier P. 1999. Tumor Necrosis
921 Factor Alpha Is a Key Mediator in the Regulation of Experimental Trypanosoma brucei
922 Infections. *Infect Immun* **67**:3128. doi:10.1128/IAI.67.6.3128-3132.1999
923 Malvy D, Chappuis F. 2011. Sleeping sickness. *Clin Microbiol Infect* **17**:986–995.
924 doi:10.1111/J.1469-0691.2011.03536.X
925 Mou Z, Jia P, Kuriakose S, Khadem F, Uzonna JE. 2010. Interleukin-17-Mediated Control of
926 Parasitemia in Experimental Trypanosoma congolense Infection in Mice. *Infect Immun*
927 **78**:5271. doi:10.1128/IAI.00168-10
928 Nogueira G, Solon C, Carraro RS, Engel DF, Ramalho AF, Sidarta-Oliveira D, Gaspar RS,
929 Bombassaro B, Vasques AC, Geloneze B, Vinolo MA, Donato Junior J, Velloso LA.
930 2020. Interleukin-17 acts in the hypothalamus reducing food intake. *Brain Behav Immun*
931 **87**:272–285. doi:10.1016/J.BBI.2019.12.012
932 Raheem KA. 2014. A Review of Trypanosomosis-Induced Reproductive Dysfunctions in
933 Male Animals. *Agrosearch* **14**:30–38. doi:10.4314/agrosh.v14i1.4
934 Schindelin J, Arganda-Carreras I, Frise E, Kaynig V, Longair M, Pietzsch T, Preibisch S,
935 Rueden C, Saalfeld S, Schmid B, Tinevez JY, White DJ, Hartenstein V, Eliceiri K,
936 Tomancak P, Cardona A. 2012. Fiji: an open-source platform for biological-image
937 analysis. *Nature Methods 2012 9:7* **9**:676–682. doi:10.1038/nmeth.2019
938 Shi L, Salamon H, Eugenin EA, Pine R, Cooper A, Gennaro ML. 2015. Infection with
939 Mycobacterium tuberculosis induces the Warburg effect in mouse lungs. *Scientific*
940 *Reports 2015 5:1* **5**:1–13. doi:10.1038/srep18176
941 Sun X, Feng X, Wu X, Lu Y, Chen K, Ye Y. 2020. Fat Wasting Is Damaging: Role of Adipose
942 Tissue in Cancer-Associated Cachexia. *Front Cell Dev Biol* **8**:33.
943 doi:10.3389/FCELL.2020.00033/BIBTEX
944 Trindade S, Rijo-Ferreira F, Carvalho T, Pinto-Neves D, Guegan F, Aresta-Branco F, Bento
945 F, Young SA, Pinto A, van den Abbeele J, Ribeiro RM, Dias S, Smith TK, Figueiredo
946 LM. 2016. Trypanosoma brucei Parasites Occupy and Functionally Adapt to the
947 Adipose Tissue in Mice. *Cell Host Microbe* **19**:837–848.
948 doi:10.1016/j.chom.2016.05.002
949 Uranga AP, Levine J, Jensen M. 2005. Isotope tracer measures of meal fatty acid
950 metabolism: Reproducibility and effects of the menstrual cycle. *Am J Physiol Endocrinol*
951 *Metab* **288**:547–555.
952 doi:10.1152/AJPENDO.00340.2004/ASSET/IMAGES/LARGE/ZH10030520040007.JPE
953 G
954 Vale PF, Jardine MD. 2015. Sex-specific behavioural symptoms of viral gut infection and
955 Wolbachia in Drosophila melanogaster. *J Insect Physiol* **82**:28–32.
956 doi:10.1016/J.JINSPHYS.2015.08.005
957 van Marken Lichtenbelt WD, Schrauwen P. 2011. Implications of nonshivering
958 thermogenesis for energy balance regulation in humans. *Am J Physiol Regul Integr*
959 *Comp Physiol* **301**:285–296.

doi:10.1152/AJPREGU.00652.2010/ASSET/IMAGES/LARGE/ZH60071176070002.JPEG

Wickham H, Averick M, Bryan J, Chang W, D' L, Mcgowan A, François R, Grolemund G, Hayes A, Henry L, Hester J, Kuhn M, Lin Pedersen T, Miller E, Bache SM, Müller K, Ooms J, Robinson D, Seidel DP, Spinu V, Takahashi K, Vaughan D, Wilke C, Woo K, Yutani H. 2019. Welcome to the Tidyverse. *J Open Source Softw* **4**:1686. doi:10.21105/JOSS.01686

Wu H, Liu G, Shi M. 2017. Interferon Gamma in African Trypanosome Infections: Friends or Foes? *Front Immunol* **8**:1105. doi:10.3389/FIMMU.2017.01105

Xiao Y, Liu D, Cline MA, Gilbert ER. 2020. Chronic stress and adipose tissue in the anorexic state: endocrine and epigenetic mechanisms. *Adipocyte* **9**:472. doi:10.1080/21623945.2020.1803643

Yao T, Deng Z, Gao Y, Sun J, Kong X, Huang Y, He Z, Xu Y, Chang Y, Yu KJ, Findley BG, Berglund ED, Wang RT, Guo H, Chen H, Li X, Kaufman RJ, Yan J, Liu T, Williams KW. 2017. Ire1a in pomc neurons is required for thermogenesis and glycemia. *Diabetes* **66**:663–673. doi:10.2337/DB16-0533/-/DC1

Yoneshiro T, Kataoka N, Walejko JM, Ikeda K, Brown Z, Yoneshiro M, Crown SB, Osawa T, Sakai J, McGarrah RW, White PJ, Nakamura K, Kajimura S. 2021. Metabolic flexibility via mitochondrial bcaa carrier slc25a44 is required for optimal fever. *Elife* **10**. doi:10.7554/ELIFE.66865

Zhang W, Cline MA, Gilbert ER. 2014. Hypothalamus-adipose tissue crosstalk: neuropeptide Y and the regulation of energy metabolism. *Nutr Metab (Lond)* **11**:27. doi:10.1186/1743-7075-11-27

Zhou X, Johnson JS, Spakowicz D, Zhou W, Zhou Y, Sodergren E, Snyder M, Weinstock GM. 2020. Longitudinal Analysis of Serum Cytokine Levels and Gut Microbial Abundance Links IL-17/IL-22 With Clostridia and Insulin Sensitivity in Humans. *Diabetes* **69**:1833. doi:10.2337/DB19-0592

Zúñiga LA, Shen W-J, Joyce-Shaikh B, Pyatnova EA, Richards AG, Thom C, Andrade SM, Cua DJ, Kraemer FB, Butcher EC. 2010. IL-17 Regulates Adipogenesis, Glucose Homeostasis, and Obesity. *J Immunol* **185**:6947. doi:10.4049/JIMMUNOL.1001269

Figure 1

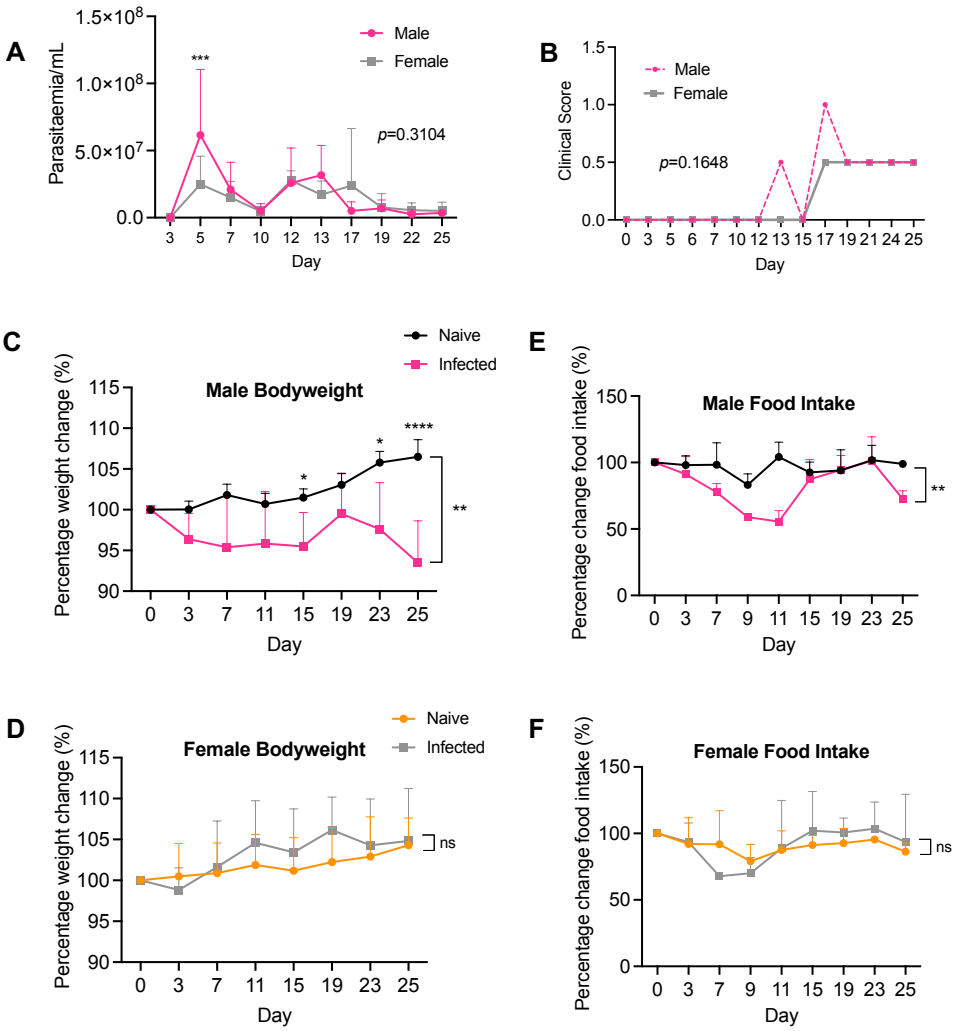
A
Parasitaemia/mL
1.5×10^8
1.0×10^8
5.0×10^7
0.0
***
Male
Female
p=0.3104
3 5 7 10 12 13 17 19 22 25
Day
B
Clinical Score
1.5
1.0
0.5
0.0
Male
Female
p=0.1648
0 3 5 6 7 10 12 13 15 17 19 21 24 25
Day
C
Naive
Infected
Male Bodyweight
Percentage weight change (%)
115
110
105
100
95
90
*
*
****
**
0 3 7 11 15 19 23 25
Day
E
Male Food Intake
Percentage change food intake (%)
150
100
50
0
**
0 3 7 9 11 15 19 23 25
Day
D
Naive
Infected
Female Bodyweight
Percentage weight change (%)
115
110
105
100
95
90
ns
0 3 7 11 15 19 23 25
Day
F
Female Food Intake
Percentage change food intake (%)
150
100
50
0
ns
0 3 7 9 11 15 19 23 25
Day

993

Figure 2

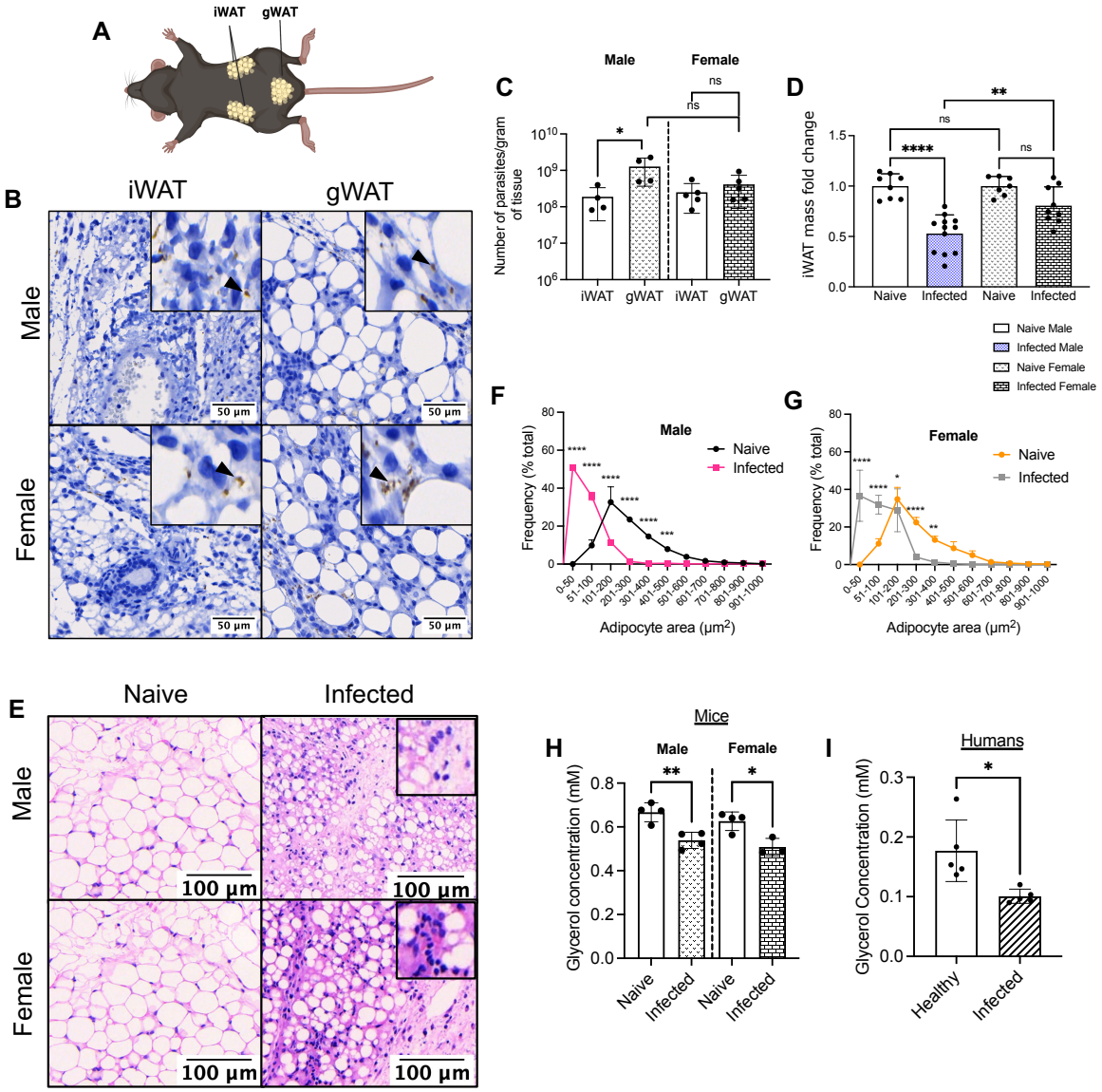
A
iWAT
gWAT
B
iWAT
gWAT
Male
Female
50 µm
C
Male
Female
ns
ns
*
Number of parasites/gram of tissue
iWAT
gWAT
iWAT
gWAT
D
**
ns
ns
****
iWAT mass fold change
Naive
Infected
Naive
Infected
Naive Male
Infected Male
Naive Female
Infected Female
F
Male
Naive
Infected
Frequency (% total)
Adipocyte area (µm²)
G
Female
Naive
Infected
Frequency (% total)
Adipocyte area (µm²)
E
Naive
Infected
Male
Female
100 µm
Mice
H
Male
Female
**
*
Glycerol concentration (mM)
Naive
Infected
Naive
Infected
I
Humans
*
Glycerol Concentration (mM)
Healthy
Infected

994

Figure 3

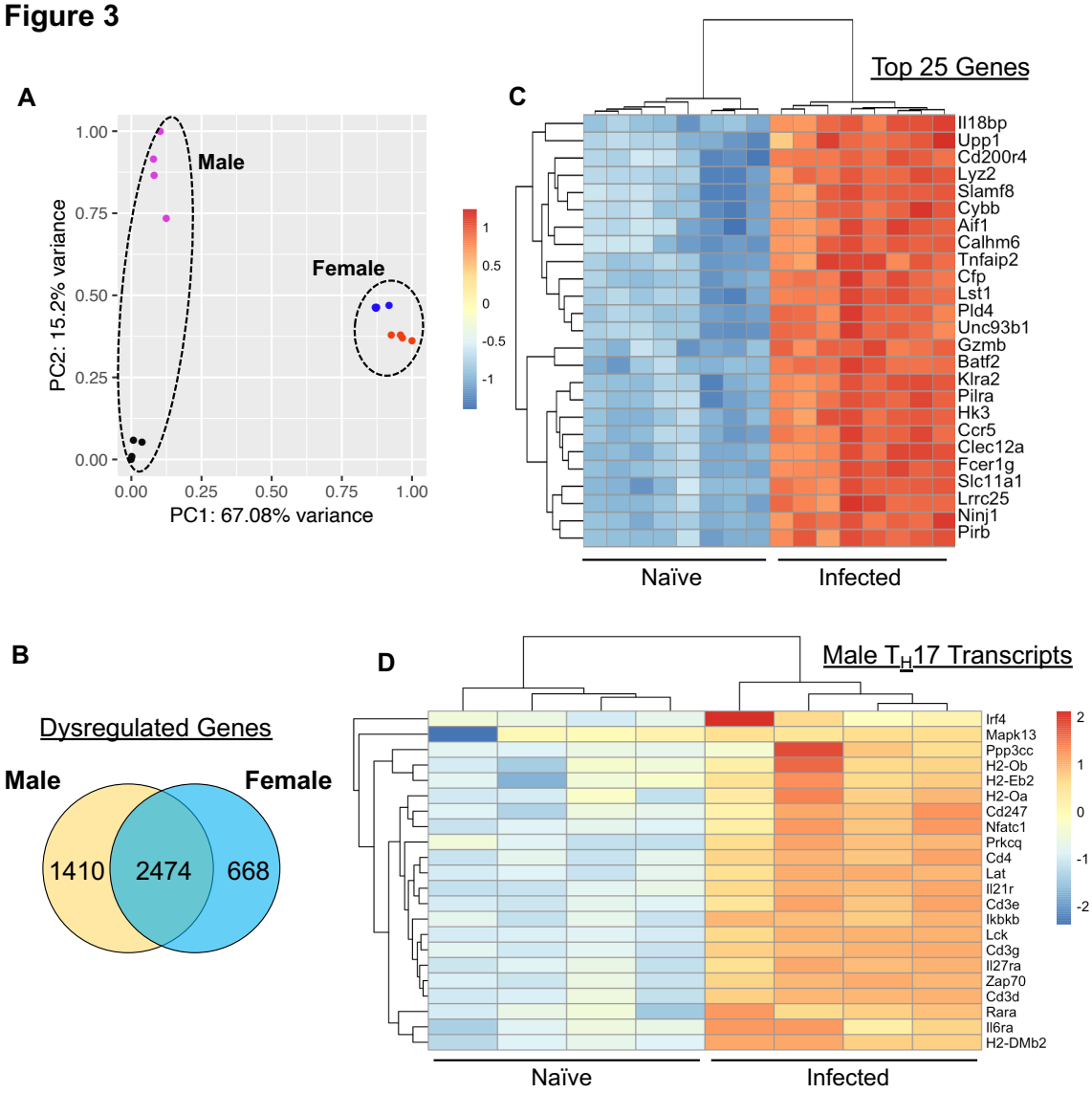
A
Male
Female
PC2: 15.2% variance
PC1: 67.08% variance
1.00
0.75
0.50
0.25
0.00
0.00
0.25
0.50
0.75
1.00
C
Top 25 Genes
Il18bp
Upp1
Cd200r4
Lyz2
Slamf8
Cybb
Aif1
Calhm6
Tnfaip2
Cfp
Lst1
Pld4
Unc93b1
Gzmb
Batf2
Klra2
Pilra
Hk3
Ccr5
Clec12a
Fcer1g
Slc11a1
Lrrc25
Ninj1
Pirb
1
0.5
0
-0.5
-1
Naïve
Infected
B
Dysregulated Genes
Male
Female
1410
2474
668
D
Male T_H17 Transcripts
Irf4
Mapk13
Ppp3cc
H2-Ob
H2-Eb2
H2-Oa
Cd247
Nfatc1
Prkcq
Cd4
Lat
Il21r
Cd3e
Ikbkb
Lck
Cd3g
Il27ra
Zap70
Cd3d
Rara
Il6ra
H2-DMb2
2
1
0
-1
-2
Naïve
Infected

995

Figure 4

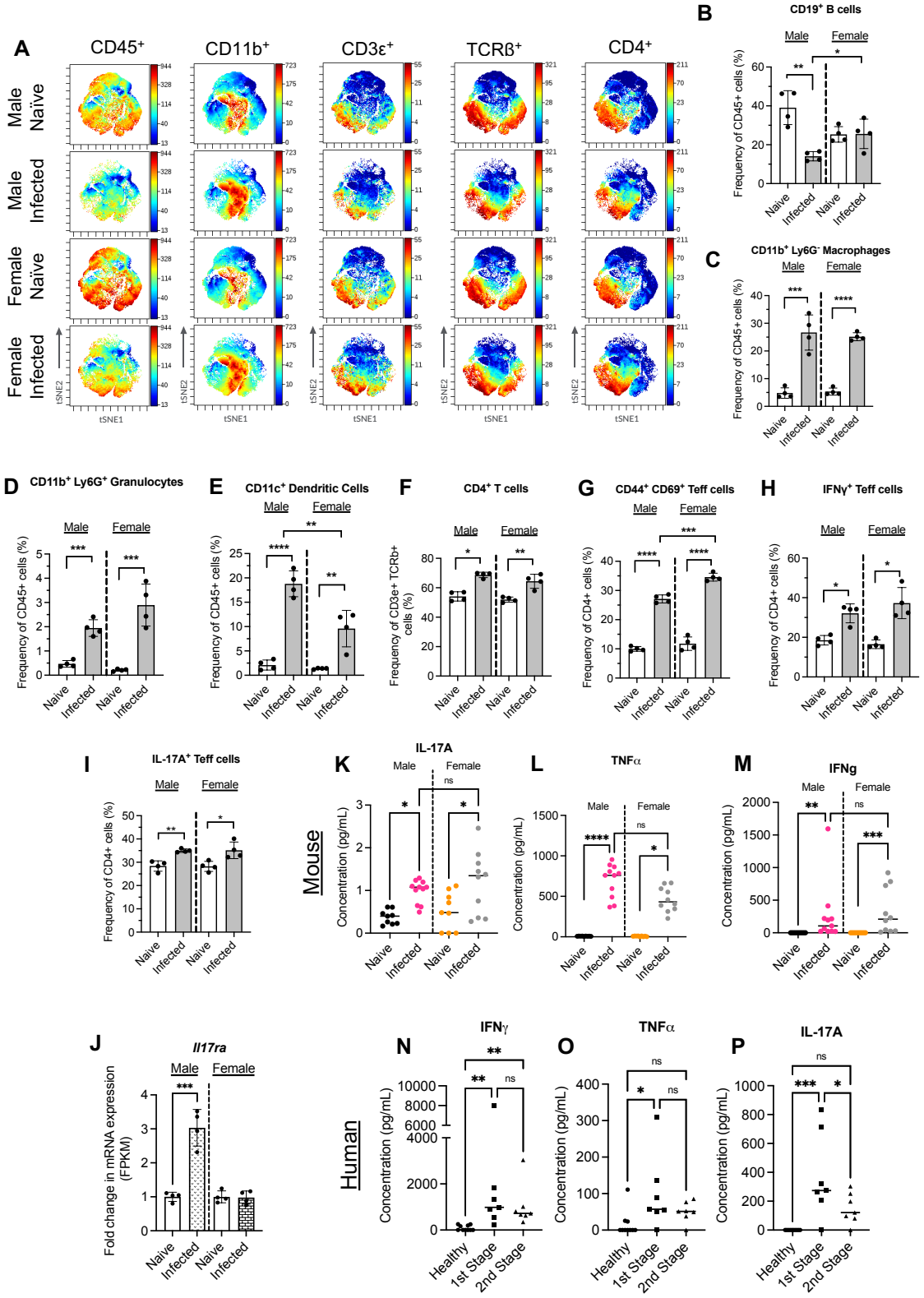
A
CD45+
CD11b+
CD3ε+
TCRß+
CD4+
Male Naïve
Male Infected
Female Naïve
Female Infected
tSNE1
tSNE2
B
CD19+ B cells
Male
Female
Frequency of CD45+ cells (%)
Naive
Infected
C
CD11b+ Ly6G- Macrophages
D
CD11b+ Ly6G+ Granulocytes
E
CD11c+ Dendritic Cells
F
CD4+ T cells
Frequency of CD3e+ TCRb+ cells (%)
G
CD44+ CD69+ Teff cells
Frequency of CD4+ cells (%)
H
IFNγ+ Teff cells
I
IL-17A+ Teff cells
J
Il17ra
Fold change in mRNA expression (FPKM)
Mouse
K
IL-17A
Concentration (pg/mL)
L
TNFα
M
IFNg
Human
N
IFNγ
O
TNFα
P
IL-17A
Healthy
1st Stage
2nd Stage
ns

996

Figure 5

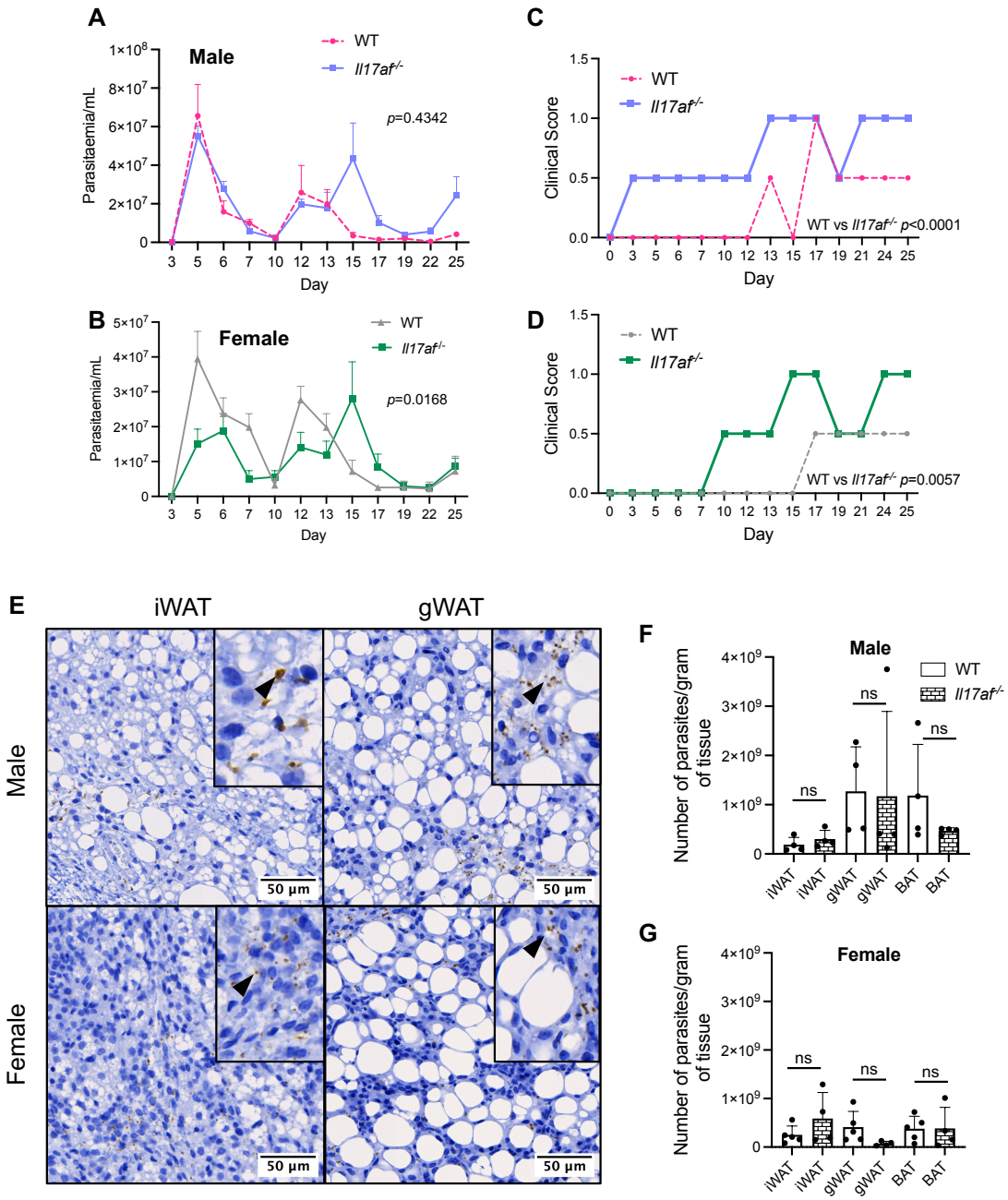
A
Male
WT
Il17af-/-
p=0.4342
Parasitaemia/mL
Day
B
Female
WT
Il17af-/-
p=0.0168
Parasitaemia/mL
Day
C
WT
Il17af-/-
Clinical Score
WT vs Il17af-/- p<0.0001
Day
D
WT
Il17af-/-
Clinical Score
WT vs Il17af-/- p=0.0057
Day
E
iWAT
gWAT
Male
Female
50 µm
F
Male
WT
Il17af-/-
Number of parasites/gram of tissue
ns
iWAT
gWAT
BAT
G
Female
Number of parasites/gram of tissue
ns
iWAT
gWAT
BAT

997

Figure 6

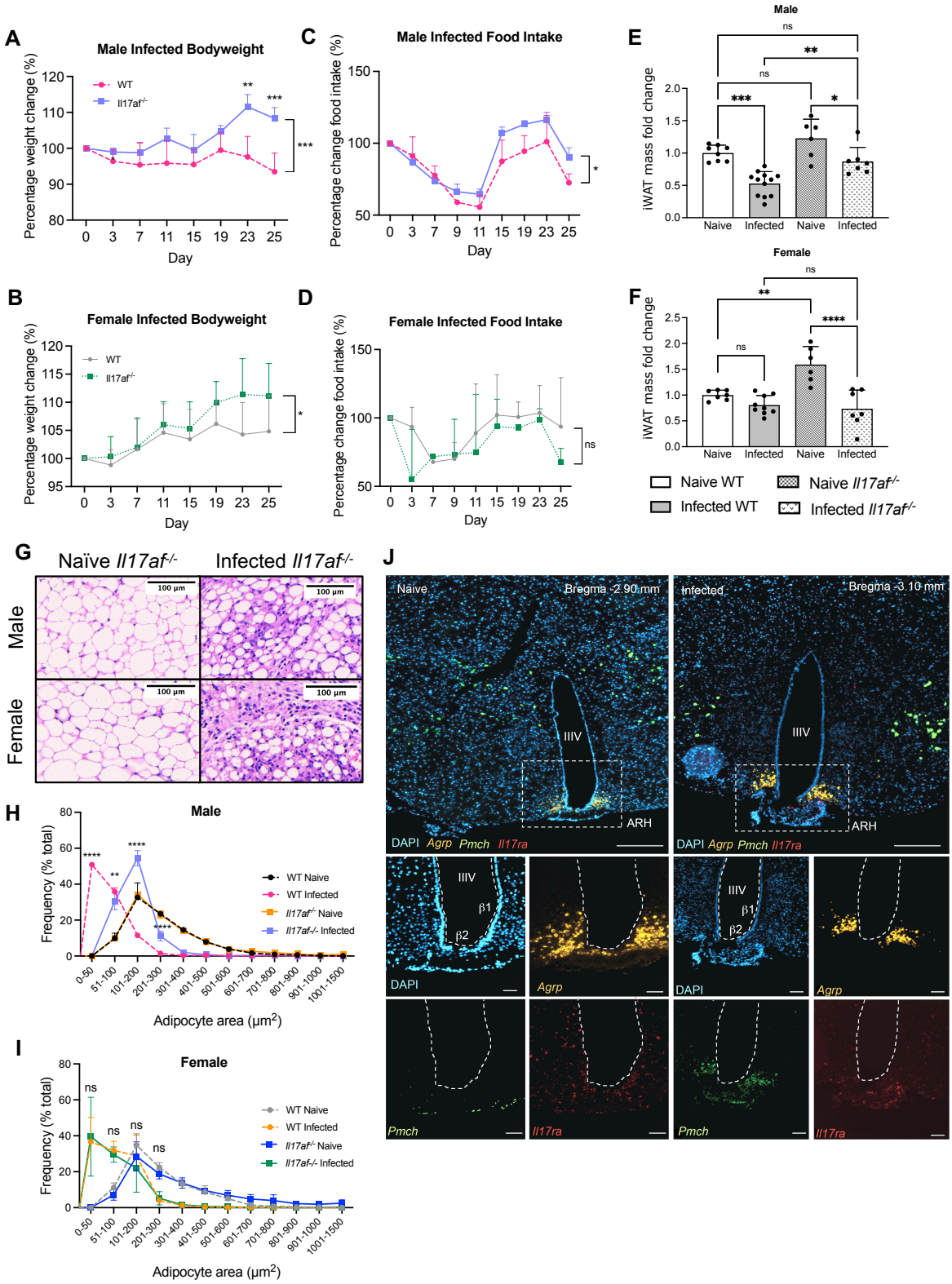

998

999